Exposure of the HIV-1 broadly neutralizing antibody 10E8 MPER epitope on the membrane surface by gp41 transmembrane domain scaffolds

Victoria Oakes, Johana Torralba, Edurne Rujas, José L. Nieva, Carmen Domene, Beatriz Apellaniz

PII: S0005-2736(18)30060-9
DOI: doi:10.1016/j.bbamem.2018.02.019
Reference: BBAMEM 82713

To appear in:

Received date: 26 October 2017
Revised date: 30 January 2018
Accepted date: 20 February 2018

Please cite this article as: Victoria Oakes, Johana Torralba, Edurne Rujas, José L. Nieva, Carmen Domene, Beatriz Apellaniz , Exposure of the HIV-1 broadly neutralizing antibody 10E8 MPER epitope on the membrane surface by gp41 transmembrane domain scaffolds. The address for the corresponding author was captured as affiliation for all authors. Please check if appropriate. Bbamem(2018), doi:10.1016/j.bbamem.2018.02.019

EXPOSURE OF THE HIV-1 BROADLY NEUTRALIZING ANTIBODY 10E8 MPER EPITOPE ON THE MEMBRANE SURFACE BY gp41 TRANSMEMBRANE DOMAIN SCAFFOLDS

Victoria Oakes[a], *Johana Torralba*[b], *Edurne Rujas*[b], *José L. Nieva*[b], *Carmen Domene*[c,d,*], *and Beatriz Apellaniz*[b,*]

[a]Department of Chemistry, Britannia House, 7 Trinity Street, King's College London, London SE1 1DB, U.K.

[b]Biofisika Institute (CSIC, UPV/EHU) and Biochemistry and Molecular Biology Department, University of the Basque Country (UPV/EHU), PO Box 644, 48080 Bilbao, Spain.

[c]Department of Chemisty, 1 South Building, Claverton Down Road, University of Bath, Bath BA2, 7AY, UK.

[d]Chemistry Research Laboratory, Mansfield Road, University of Oxford, Oxford OX1 3TA, U.K.

*Corresponding authors:

Beatriz Apellaniz, Departamento de Fisiología, Facultad de Farmacia, Universidad del País Vasco (UPV/EHU), Paseo de la Universidad, 7, 01006 Vitoria-Gasteiz, Spain. Telephone: 0034 94 5013438. E-mail: beatriz.apellaniz@ehu.eus

Carmen Domene, Department of Chemistry, 1 South Building, Claverton Down Road, University of Bath, Bath BA2 7AY, UK. E-mail: C.Domene@bath.ac.uk

Abbreviations: MPER, membrane-proximal external region; TMD, transmembrane domain; Env, HIV-1 envelope glycoprotein; molecular dynamics (MD); bNAb, broadly neutralizing antibody; CDR-H3, complementarity-determining region three of the heavy chain; HC, heavy chain; WT, wild-type; pBPA, p-benzoylphenylalanine; DMPC, 1,2-dimyristoyl-*sn*-glycero-3-phosphocholine; DHPC, 1,2-dihexanoyl-*sn*-glycero-3-phosphocholine; Chol, cholesterol; POPC, 1-palmitoyl-2- oleoyl-sn-glycero-3-phosphocholine; PA, L-α-phosphatidic acid, POPA, 1-palmitoyl-2-oleoyl-*sn*-glycero-3-phosphate; Rho-PE, 1,2-dioleoyl-*sn*-glycero-3-phosphoethanolamine-N-(lissamine rhodamine B sulfonyl); CD, circular dichroism; HFIP, 1,1,1,3,3,3-hexafluoro-2-propanol; N_P, number of atomic interaction pairs; MAb4E10, monoclonal antibody 4E10; HRP, horseradish peroxidase.

Abstract

The 10E8 antibody achieves near-pan neutralization of HIV-1 by targeting the remarkably conserved gp41 membrane-proximal external region (MPER) and the connected transmembrane domain (TMD) of the HIV-1 envelope glycoprotein (Env). Thus, recreating the structure that generates 10E8-like antibodies is a major goal of the rational design of anti-HIV vaccines. Unfortunately, high-resolution information of this segment in the native Env is lacking, limiting our understanding of the behavior of the crucial 10E8 epitope residues.

In this report, two sequences, namely, MPER-TMD1 (gp41 residues 671-700) and MPER-TMD2 (gp41 residues 671-709) were compared both experimentally and computationally, to assess the TMD as a potential membrane integral scaffold for the 10E8 epitope. These sequences were selected to represent a minimal (MPER-TMD1) or full-length (MPER-TMD2) TMD membrane anchor according to mutagenesis results reported by Yue et al. (2009) *J. Virol.* 83, 11588. Immunochemical assays revealed that MPER-TMD1, but not MPER-TMD2, effectively exposed the MPER C-terminal stretch, harboring the 10E8 epitope on the surface of phospholipid bilayers containing a cholesterol concentration equivalent to that of the viral envelope. Molecular dynamics simulations, using the recently resolved TMD trimer structure combined with the MPER in a cholesterol-enriched model membrane confirmed these results and provided an atomistic mechanism of epitope exposure which revealed that TMD truncation at position A700 combined with N-terminal addition of lysine residues positively impacts epitope exposure. Overall, these results provide crucial insights into the design of effective MPER-TMD derived immunogens.

Key words: Molecular dynamics simulation; transmembrane domain; antigenicity; vaccine development; HIV-1.

1. Introduction

The HIV-1 envelope glycoprotein (Env) is a class I viral fusion glycoprotein that initiates the infection cycle and the only protein on the viral particle accessible to the immune system. Since the publication in 2013 of the high-resolution cryo-EM [1] and x-ray [2] structures of the clade A BG505 strain SOSIP construct, a stabilized soluble prefusion Env trimer cleaved at position D664, several other native-like structures from the same [3] and other clades [4, 5] have been reported and have provided detailed information on the architecture of the native gp41 ectodomain (for a comprehensive review of the available Env structures, see [6]). By comparison, less is known on the structure-function relationships regarding the MPER and TMD sequences after position D664. Besides its structural role in anchoring the Env complex to the viral membrane [7, 8], the MPER-TMD region is required for cell-cell fusion, viral infectivity and immunosuppression [9-18]. Moreover, the highly conserved MPER sequence constitutes a vulnerability site on the Env complex targeted by broadly neutralizing antibodies (bnAbs) [19-22]. Specifically, antibodies directed against the MPER C-terminal helix, such as 4E10 or 10E8, display near pan-neutralization activity in standard panels of HIV strains and isolates [23, 24]. Since 10E8 is a more potent antibody that lacks polyreactivity, ongoing immunogen-design strategies target this antibody [19, 22, 25].

In this regard, previous studies suggested that the neutralization-competent structure of the MPER might also implicate part of the native TMD sequence [13, 26-29]. Accordingly, 4E10 and 10E8 bnAbs bound to MPER expressed on the surface of the plasma membrane with significantly higher affinity when tethered to it via the TMD of HIV-1 gp41, rather than via the platelet-derived growth factor receptor TMD [26]. Supporting the involvement of the TMD in MPER antigenicity, we have recently reported NMR [28] and x-ray structural data [30] indicating that the C-terminal half of the MPER and the N-terminal half of the TMD (MPER-N-TMD) arrange into a continuous helix spanning residues 673 to 690. This observation was reinforced by the publication of a NMR structure of a HIV-1 clade D TMD trimer (isolate 92UG024.2, residues 677-716, HXB2 numbering) in DMPC:DHPC (1:2, mol:mol) bicelles

[13]. Together, these results oppose the long-standing hypothesis that the helix bends at the MPER-TMD connection (residue K683) to allow TMD insertion into the membrane in an orientation perpendicular to the bilayer plane [31, 32]. In accordance with the experimental evidence, we hypothesized that the unbent MPER-N-TMD helix might function as a scaffold to increase the affinity of anti-MPER antibodies at membrane surfaces [28] and found that indeed, the complete 10E8 epitope includes TMD residues beyond K683 [30].

In this work, we analyze the effect of elongating the continuous MPER-N-TMD α-helix towards the TMD C-terminus on the exposure of the 10E8 MPER epitope at membrane surfaces (Fig. 1). To this end, immunochemical assays and molecular dynamics (MD) simulations have been employed to analyze the potential of MPER-TMD derived sequences of different lengths to scaffold the 10E8 epitope when incorporated into liposomal vaccines with a cholesterol concentration that matches that of the viral envelope [33]. Moreover, the effect on epitope exposure of N- and/or C-terminal positive charge addition is analyzed. Our findings have the potential to aid the development of new vaccine formulations that effectively elicit the production of 10E8-like anti-MPER antibodies.

2. Materials and Methods

2.1 Materials

Synthetic peptides derived from the gp41 MPER-TMD, *KKK*-^{671}NWFDITNWLWYIKLFIMIVGGLVGLRIVFA^{700}-*KKKK* (MPER-TMD1) and ^{671}NWFDITNWLWYIKLFIMIVGGLVGLRIVFAVLSVVNRVR^{709} (MPER-TMD2) were produced by solid-phase synthesis using Fmoc chemistry as C-terminal carboxamides and purified by HPLC. 1-palmitoyl-2-oleoyl-*sn*-glycero-3-phophocholine (POPC), L-α-phosphatidic acid (Egg, Chicken) (PA), cholesterol (Chol), and 1,2-dioleoyl-*sn*-glycero-3-

phosphoethanolamine-N-(lissamine rhodamine B sulfonyl) (Rho-PE) were purchased from Avanti Polar Lipids. Goat anti-Human IgG (Fab specific) was obtained from Sigma-Aldrich, rabbit anti-Human IgG-HRP and mouse anti-goat IgG-HRP from Santa Cruz Biotechnology. Monoclonal antibody 4E10 (MAb4E10) was kindly donated by D. Katinger (Polynum Inc., Vienna, Austria). 4E10 and 10E8 wild type Fabs, their non-functional mutant versions and their Trp100b$_{HC}$*p*BPA substituted versions were produced as previously described [27, 30].

2.2 Circular Dichroism

Circular dichroism (CD) measurements were obtained from a thermally controlled Jasco J-810 circular dichroism spectropolarimeter calibrated routinely with (1S)-(+)-10-camphorsulfonic acid, ammonium salt. Samples consisted of lyophilized synthetic peptides dissolved at concentrations of 0.03 mM in 2 mM Hepes (pH, 7.4) buffer containing 25 % (v/v) of the low-polarity organic solvent 1,1,1,3,3,3-hexafluoro-2-propanol (HFIP). Spectra were measured in a 1 mm path-length quartz cell initially equilibrated at 25 ºC. Data were taken with a band-width of 1 nm at 100 nm/min speed, and the results of 20 scans were averaged.

2.3 Peptide reconstitution into liposomes

To ensure proper incorporation of the peptides into the vesicles, lipids and peptides (MPER-TMD1 and MPER-TMD2) were mixed in organic solvent prior to the production of the liposomes. Briefly, POPC, Chol and PA were dissolved in chloroform:methanol 1:2 (vol:vol) at 10:11:1 (mol:mol) ratio and were mixed with MPER-TMD1 or 2 (dissolved in % 100 ethanol) to achieve a peptide-to-lipid molar ratio of 1:50. The mixture was dried under a N_2 stream and traces of organic solvents were removed by 2 h vacuum pumping. Subsequently, the dried lipid films were subjected to 2 h of gentle hydration with H_2O using a N_2 gas bubbler to facilitate the subsequent dispersion of the dried lipid-peptide film in PBS aqueous buffer. Next, the multilamelar vesicles were bath sonicated (1 h, 55 ºC) and subjected to 15 freeze and thaw cycles to obtain unilamelar vesicles. Chol concentration of liposome suspensions was determined by the cholesterol oxidase/peroxidase method

(BioSystems, Barcelona, Spain), and found to be within the experimental error.

2.4 Liposome flotation assay

Following the method described by Yethon *et al*. [34], vesicle flotation experiments in sucrose gradients were performed to assess the association of 4E10 and 10E8 Fabs or their mutant counterparts to their epitopes presented by the MPER-TMD1 or MPER-TMD2 scaffolds in cholesterol-enriched membranes. In brief, 200 µL of a sample containing rhodamine-labeled liposomes (1.5 mM lipid concentration, 0.5 mol % Rho-PE)) and peptide (30 µM peptide; 1:50 peptide-to-lipid molar ratio) was incubated with Fabs for 15 min at RT under constant stirring (800 rpm). 100 µL of the sample was adjusted to a sucrose concentration of 1.4 M in a final volume of 300 µL, and subsequently overlaid with 400 µL- and 300 µL-layers of 0.8 M and 0.5 M sucrose, respectively. The gradient was centrifuged at 436,000 $\times$ g for 3 h at 4 ºC in a TLA 120.2 rotor (Beckman Coulter). After centrifugation, four 250 µL-fractions were collected. Material adhered to tubes was collected into a 5th fraction by washing with 250 µL of hot (100 ºC) 1 % (w/v) SDS. The presence of MPER-TMD truncated peptides and Fabs in the different fractions and in the original sample (input) was revealed by Western Blot analysis after Tris-Tricine SDS-PAGE separation. MAb4E10 (0.05 µg/ml) and rabbit anti-human-IgG-HRP, and goat anti-Human IgG (Fab specific) and mouse anti-goat IgG-HRP antibody pairs were used to reveal peptides and Fabs, respectively. The presence of liposomes in the different fractions was determined after measuring the fluorescence emission of the Rho-PE probe [12].

2.5 Photo-cross-linking assay

For the photo-cross-linking experiments, samples containing 1.5 µM Fab bearing the 10E8 or 4E10 W100b$_{HC}$*p*BPA substitution and 30 µM of peptides MPER-TMD1 or MPER-TMD2 in solution (PBS) or reconstituted into membranes (1.5 mM lipid) were incubated for 15 min at RT and irradiated afterwards with UV light at 365 nm for 20 min at 4 °C, using a UVP B-100AP lamp. Finally, Fab heavy-chain-peptide adducts were separated by 15 % Tris-Glicine

SDS-PAGE and stained with Coomassie blue.

2.6 Molecular Dynamics Simulations

The atomic structures of the HIV-1 gp41 TMD trimer (PDB ID: 5JYN) [13] and the MPER-N-TMD helix (PDB ID: 5GHW) [30] were superposed to create models of peptide trimers representing the MPER-TMD region with or without C-terminal truncations, and with or without N- and/or C-terminal lysine residues. Residues 671 to 689 were extracted from 5GHW, with residues from 690 onwards obtained from 5JYN, to ensure agreement between the peptide sequences used experimentally and computationally.

The N-termini of the peptides were modeled in a charged state whilst the C-termini were amidated. Default protonation states were used for ionizable residues. Water molecules were manually added to the region surrounding the protonated R696, in keeping with the presence of structured water molecules noted by Dev et al. [13]. Peptide assemblies MPER-TMD1 (no lysines, N-terminal lysines, C-terminal lysines, and N- and C- terminal lysines), and MPER-TMD2 (no lysines), were inserted into model membranes, containing POPC, POPA and cholesterol molecules in a 10:11:1 ratio, using the CHARMM-GUI Membrane Builder [35-37]. For this purpose, the replacement method was utilized. In this approach, pseudo atoms representing lipids are distributed around the protein, and replaced with molecules randomly selected from the associated lipid molecule library [35]. The system was solvated with approximately ~30,000 water molecules, with added NaCl to mimic to the 150 mM experimental concentration and achieve neutralization. NAMD2.9 was employed to perform MD simulations [38]. The CHARMM36 force field was used to describe the peptide and lipids [39], the TIP3P model for water [40], and standard parameters were used for ions [41]. The Particle Mesh Ewald method was used for the treatment of periodic electrostatic interactions, with an upper threshold of 1 Å for grid spacing [42]. Electrostatic and van der Waals forces were calculated every time step. A cut-off distance of 12 Å was used for van der Waals forces. A switching distance of 10 Å was chosen to smoothly truncate the non-

bonded interactions. Only atoms in a Verlet pair list with a cut-off distance of 14 Å (reassigned every 20 steps) were considered [43]. The SETTLE algorithm was used to constrain all bonds involving hydrogen atoms to allow the use of a 2 fs time step throughout the simulation [44]. The Nose-Hoover-Langevin piston method was employed to control the pressure with a 200 fs period, 50 fs damping constant and a desired value of 1 atmosphere [45, 46]. The system was coupled to a Langevin thermostat to sustain a temperature of 298 K throughout. Systems were minimized for 1000 steps, and then subject to 4 ns of constrained dynamics to equilibrate. Four equilibration steps of 1 ns were performed, with restraints (force constant: 1 kcal/mol) imposed on different elements of the system to ensure gradual relaxation of the system; 1) protein atoms, lipid head groups, and water molecules within the trimer pore and in contact with R696 are restrained, in order to relax lipid tails and water molecules in the vicinity of the lipid headgroups; 2) protein atoms and water molecules within the trimer pore and in contact with R696 are restrained, so lipid molecules can adjust to the protein surface; 3) only protein atoms are restrained, to ensure internal water molecules, and those in contact with R696 residues, occupy the most energetically unfavourable positions; 4) protein backbone atoms are restrained, to allow optimisation of side-chain dynamics. Unconstrained dynamics was then performed for 200 ns. Analysis was performed using in-house TCL scripts for VMD [47].

3. Results

3.1 Design of the MPER-TMD1 and MPER-TMD2 peptide scaffolds

Figure 1A describes the two sequences derived from the MPER-TMD region that were designed to upgrade our previous vaccines based on the MPER-N-TMD sequence (termed CpreTM in our recent work) [28]. To that end, these sequences included different sections of the native TMD sequence, due to the previously reported positive effect in 4E10 and 10E8 antibody binding to their epitopes [30, 48]. The MPER-TMD1 sequence encompasses Env

residues ^{671}**NWF**DI**T**NWL**W**YI**K**LFIMIVG*GLVGLRIVFA*^{700} (sequence numbering derived from the prototypic HXBc2 isolate) and embodies the unbent MPER-N-TMD helix (residues 673 to 690, underlined) [28, 30] including the complete 10E8 epitope sequence (critical residues in bold) [24, 30, 49], which has been elongated to include part of the C-terminus of the TMD (in italics). The TMD portion in this sequence has been truncated at position A700 according to mutagenesis results reported by Yue *et al.* [9]. This mutant was found to represent a minimal TMD anchor, which allowed efficient transport of Env to the plasma membrane, and wild-type levels of cell-cell fusion [9]. Finally, three and four lysine residues were added to this sequence at the N- and C-termini, respectively, to match the hydrophobicity of our previously reported CpreTM sequence [28]. The MPER-TMD2 sequence (Env residues, ^{671}**NWF**NI**T**NWL**W**YI**K**LFIMIVG*GLVGLRIVFAVLSLVNRVR*^{709}) bears the 10E8 epitope (critical residues in bold), the MPER-N-TMD helix sequence (underlined) and the sequence assumed to span the full TMD (in italics) [50], which contains the minimal number of amino acids required for WT-like incorporation of Env and some degree of infectivity [9].

3.2 Experimental assessment of the antigenicity of MPER-TMD scaffolds

3.2.1 Secondary structure

Following synthesis, the secondary structures of MPER-TMD1 and MPER-TMD2 peptides were compared by circular dichroism in the low-polarity organic solvent HFIP that roughly mimics the membrane environment. As shown in figure 1B, the synthetic peptides adopted similar levels of α-helical conformation, as expected from previous structural studies [13, 28], underpinning their further comparison as synthetic surrogates of the MPER-TM domain.

3.2.2 Incorporation into membranes and antigenicity

Next, we tested experimentally the capacity of the synthetic peptides to incorporate into cholesterol-enriched bilayers and expose the 10E8 MPER epitope at membrane surfaces. In those assays, MPER-TMD1 and MPER-TMD2 (Figs. 2A and 2B, respectively, 10 kDa panels) mostly co-floated with lipid vesicles (rhodamine emission spectra) upon physical

separation of bound and unbound species by ultracentrifugation in a sucrose gradient. The absence of peptide in the SDS and 1st fractions (non-floated fractions) further confirmed that both peptides were effectively incorporated into vesicles containing 50 mole % cholesterol. The appropriate display (antigenicity) of the 10E8 bnAb epitope in the MPER-TMD peptides reconstituted into membranes was subsequently assayed (Fig. 2). To this end, the binding capacity of the reconstituted MPER-TMD petides to a functional (neutralizing) wild type 10E8 Fab (Fig. 2, left panels) and to a non-functional (non-neutralizing) mutant Fab (Fig. 2, right panels) was compared. The 10E8 mutant Fab, termed 10E8 W100bD, was obtained by decreasing the hydrophobicity of the CDR-H3 loop after substitution of the critical tryptophan residue 100b of the CDR-H3 apex with Asp, a mutation that abrogates neutralization and binding to the epitopes in a membrane milieu [30]. Therefore, it comprises a valuable tool to discriminate functional and non-functional binding to the liposome-peptide formulations proposed as immunogens. The 10E8 wild type Fab, but not the W100bD mutant, effectively recognized the MPER-TMD1 peptide in the membrane, demonstrated by the 25 kDa bands corresponding to the Fab, co-floating with the liposomes bearing the peptide (Fig. 2A, left panel). This result reveals the capacity of MPER-TMD1 reconstituted into cholesterol-enriched vesicles to effectively expose the epitope of the 10E8 bnAb following a neutralization-competent pattern. In contrast, both wild type and mutant Fabs were recovered from the non-floated fractions when the epitope was presented by the MPER-TMD2 peptide in the surface of the liposomes (Fig. 2B) or when the epitope was absent (Fig. 2C). Overall, these results are consistent with the correct exposure of the epitope in the MPER-TMD1 scaffold when reconstituted into cholesterol-enriched liposomes and reveal its potential as an immunogen to elicit 10E8-like anti-MPER antibodies.

To determine whether the observed difference in antigenicity between the two MPER-TMD scaffolds was specific to the 10E8 antibody or could be reproduced with other anti-MPER antibodies, the same experiment was performed with Fab 4E10, whose epitope maps to the same region [24, 51]. As shown in figure S1, wild type 4E10 Fab recognized and bound to

MPER-TMD1 reconstituted into liposomes (Fig. S1A, left panel), but was recovered from the non-floating fractions either when the epitope was presented by the MPER-TMD2 scaffold (Fig. S1B, left panel) or in the absence of the epitope (Fig. S1C, left panel). Following the same strategy used with 10E8, a non-functional (non-neutralizing) 4E10 mutant Fab was also assayed to determine the relevance of the MPER-TMD1 scaffold as immunogen. This mutant, termed 4E10 Δloop, has an intact paratope while the tip of the CDR-H3 loop is ablated. Preservation of this loop is required for neutralization [27] but its deletion has a negligible effect on Fab binding to the epitope in solution, displaying near wild type affinity [49]. Similarly to 10E8 W100bD and in contrast to 10E8 or 4E10 wild type Fabs, 4E10 Δloop binding to MPER-TMD scaffolds reconstituted in a membrane was barely detected (Fig. S1, right panels). Together, these data suggest that the C-terminal MPER epitope targeted by these bnAbs is not properly exposed in the MPER-TMD2 scaffold.

Binding assays were next complemented with photo-cross-linking experiments. This approach allows scoring effective engagement of the epitope peptide with the antibody in an intact system [48] and serves to rule out the possibility that the antibodies bound to MPER-TMD2, but would dissociate during the ultracentrifugation protocol (Fig. 3). To carry out the experiment, the UV-sensitive unnatural amino acid *p*-benzoylphenylalanine (*p*BPA) [52, 53], was genetically encoded at position Trp100b of the 10E8 Fab heavy chain (HC) CDR-H3 tip. Following incubation of the modified Fab with either MPER-TMD1 or MPER-TMD2 in solution or reconstituted into membranes, the samples were subjected to UV light, and the formation of covalent adducts analyzed by SDS-PAGE. As expected, an additional band corresponding to cross-linked peptide and Fab 10E8 HC was observed in MPER-TMD1 containing samples, both in solution and in liposomes, but not in samples containing MPER-TMD2 in liposomes, consistent with the flotation assay. However, a shift in the gel was also observed in MPER-TMD2 samples devoid of a lipid membrane, indicating that correct exposure of the epitope is reliant on its environment, with membrane insertion hindering recognition of the epitope by the anti-MPER antibody. The new band was absent in all cases

before irradiation (UV^- lines) and in the absence of the epitope, demonstrating that UV-mediated cross-linking specifically causes the appearance of this band.

Flotation and photo-cross-linking experiments also revealed that MPER-TMD1 migrated on tricine-SDS-PAGE with an apparent molecular weight of 10 kDa (theoretical MW of 4.5 kDa for MPER-TMD1) revealing the potential of this peptide to form stable dimers even in the harsh conditions of the experiments (5 min at 100 ºC and 1 % SDS). On the contrary, MPER-TMD2 migrated as two bands, compatible with dimers and trimers, suggesting formation of stable higher-order oligomers in cholesterol-enriched membranes. This differential behavior might have implications in the effective exposure of the MPER epitope at the membrane surface.

3.3 Molecular Dynamic Simulations of MPER-TMD derived peptide scaffolds

3.3.1 Construction of the models

To understand the molecular mechanism underlying the above experimental observations, molecular dynamics (MD) simulations of the MPER-TMD1 and MPER-TMD2 peptides inserted into HIV-1-like cholesterol-enriched membranes were performed. The starting models (Fig. 4A) were constructed by superposition of the MPER-N-TMD structure (PDB ID: 5GHW), residues 671-689, with residues 690-700 or 690-709 of the individual helices of the recently resolved TMD trimer (PDB ID: 5JYN), to form MPER-TMD1 and MPER-TMD2, respectively. As described earlier, synthetic peptides and lipids were mixed in organic phase to produce liposomal vaccines; peptides were not added to preformed liposomes from the aqueous phase. Moreover, the free energy change of transferring residues from 671 to 693 from interface to octanol is negative [54] and residues downstream K683 have a hydrophobicity profile compatible with that of a membrane-buried sequence [55]. Thus, rather than laying on the bilayer surface parallel to the plane of the membrane, the trimers were inserted into the membrane assuming in both cases a disposition parallel to the bilayer normal (Fig. 4A). MD simulations were performed for 200 ns (Fig. 4B), with the initial 100 ns

period considered an equilibration period. Therefore, only the final 100 ns of the simulations is considered in the analysis presented hereafter.

3.3.2 Overall stability of the models

Firstly, the root-mean-square deviation (RMSD) of the Cα atoms from the initial structure was monitored over time to assess the stability of the epitope region in the MPER-TMD derived constructs (Fig. 5A). The RMSD of MPER-TMD1 (4.4 ± 0.3 Å) is significantly higher than that of MPER-TMD2 (2.3 ± 0.2 Å), suggesting the assemblies adopt different configurations, with the latter resembling the initial construct most closely, based upon the NMR structure of the HIV-1 TMD and demonstrated by the calculated number of interaction pairs between adjacent helices (Fig. 5B) in each assembly. 300 to 450 atomic interaction pairs are present between adjacent helical pairs (CA > BC > AB) in MPER-TMD2, suggesting a near-symmetrical trimer assembly. An interaction number of this magnitude is only observed for the AC helix pair in MPER-TMD1, with the remaining number of pairwise interactions considerably reduced, to 237 and 118 between helices AB and BC, respectively. These observations suggest that the MPER-TMD1 trimer is unstable and might dissociate in a cholesterol-enriched bilayer, in agreement with earlier experimental results establishing the existence of MPER-TMD1 dimers (Fig. 2).

Moreover, inspection of the transmembrane helix tilt angle (τ) for residues 671-690, relative to the bilayer normal, showed noticeable differences between the trimers (Fig. 5C). At the beginning of the simulation (0 ns) helices A, B and C displayed tilt angles of 15.2°, 18.4° and 25.3°, respectively. In the last 100 ns of the simulation, helices A and B of the MPER-TMD2 trimer occupy a similar range, between 8-14º relative to the bilayer normal, whereas helix C fluctuates between 17-20°. Therefore, all of them display an increased verticality as compared to the initial model. In contrast, helices B and C of MPER-TMD1 display tilt angles of ca. 16° and 28°, equivalent to the initial model, whilst the tilt angle of helix A increases to

ca. 24º. This result suggests that the assembly of the transmembrane trimer is noticeably perturbed.

3.3.3 Specific molecular interactions that define the observed conformations

To gain further insight at the molecular level into the interactions that contribute to the stabilization of the constructs in the simulations, we next analyzed the contacts between specific amino acids in each assembly and with the lipid bilayer. Specific interaction pairs are considered to be relevant if the number of atomic interaction pairs, $N_{P,}$ is greater than 15. As the MPER-TMD1 structure is no longer symmetric, no residue pairs are identified with an average N_P of more than 15 (Fig. 6A). Deconstruction of the MPER-TMD1 contact map into individual pairs of helices (Fig. 6B), identifies a prominent contact interface between monomers A and C, incorporating residue pairs W672-W680, I675-W680, W672-K683, L679-K683, L679-I686, L679-M687, I682-M687, I686-I693 and V689-I697 (N_P > 15), with L679-K683 and L679-M687 being the most prominent contacts (N_P > 25). This implies that monomers A and C shift relative to one another (region W672-V689 of A interacts with region W680-I697 of C) due to the increased tilt angle of helix A. On the other hand, region K683-I693 of monomer B interacts with region I686-R696 of A via residue pairs, K683-I686, M687-I686, I686-I693, M687-V689, G690-I693, I693-I693, and I693-R696 (N_P > 15), with I686-I693 and I693-R696 being the most prominent pairs identified. Finally, no residue pairs are identified (with N_P > 15) between monomer B and C. These results indicate that MPER-TMD1 contains two energetically favorable dimer interfaces, between the N-terminal regions of helices A and C and the C-terminal regions of A and B.

In contrast, in the MPER-TMD2 simulation, inter-helical interactions span the region between W678 and I697 with several residue pairs identified with N_P > 15 (Fig. 6C). Residue pairs W678-L679, I682-K683, F685-M687, F685-I686, I686-I686, L692-I693, I693-I693, and R696-I697 exceed this value, when averaged over the three helices. In this case, deconstruction of the MPER-TMD2 contact map into individual pairs of helices reveals that similar residues

participate in pairwise interactions (Fig. 6D) consistent with the near-symmetrical conformation of the trimer. Overall, residues I686 and I693 corresponding to the *a* and *d* positions of the coiled-coil, are involved in 32 % and 26 % of the total number of interaction pairs, and thus, contribute to the stability of the trimer to the greatest extent.

Regarding interactions with lipids, residues K668 and W680 populate the head group region of the upper leaflet in helix A and residues K668 and K670 in helix C of the MPER-TMD1 simulation, whereas W672, F673 and W678 occupy this region in helix B (Fig. 7A). In the lower leaflet, C-terminal lysine residues inhabit the head group region in all helices, and also R696 in helix A, despite residing in the hydrophobic core. Critical residues that anchor the peptide to the hydrophobic membrane core, common to all helices, include Y681, L684, F685, I688, L692 and L695 (Fig. 7B). However, several differences between the helices are observed regarding acyl chain interactions, with W678 displaying an elevated number of interactions with the acyl chains in helices A and C, and W680 and M687 in helix B. Moreover, it's worth noting that C-terminal residues in helix C unfold to facilitate snorkeling of lysines 700 to 704 and to permit accommodation of the hydrophobic residues to the thickness of the bilayer (Fig. 1C). Similarly, helix A unfolds to accommodate the helix to the thickness of the hydrophobic core, in this case between residues G694 and V698. Helix B, which is less tilted, spans the membrane without unfolding. In the case of the MPER-TMD2 simulation, residues W680 and R709 in all three helices consistently populate the head group region of the upper and lower leaflets, respectively. Furthermore, besides the residues described to interact with the acyl chains in MPER-TMD1, interactions between residues M687, S691, I697, V698, F699, V701 and V702 and the hydrophobic core of the membrane were also recorded.

3.3.4 Accessibility of the 10E8 epitope residues

To assess accessibility of the epitope within the MPER-TMD scaffolds, the average number of atomic interactions of the main epitope residues, N671, W672, F673, T676, W680 and

K683, with other protein residues was calculated (Table 1). These residues display approximately 100 interactions in MPER-TMD1 helix A, mainly resulting from W672 and K683. In helix B, the number of interactions is at a minimum, with K683 involved in an average of 8 interaction pairs and no interactions recorded for the other residues. Hence, the 10E8 epitope in helix B retains a large surface area to interact with other species. However, epitope residues in this helix are engaged in extensive lipid interactions (Fig. 7 and Table 2); W672 and F673 interact with the phospholipid head groups, and W680 and, to a lesser extent K683, interact with the hydrophobic core. In helix C, protein residues occlude the lower region of the epitope, with W680 and K683 involved in ca. 120 interaction pairs. In contrast, N-terminal epitope residues N671, W672 and F673 are not engaged in interactions with other residues or surrounding lipid molecules. Thus, the N-terminal part of helix C in MPER-TMD1 is exposed to the solvent and might effectively interact with the antibody.

Conversely, epitope residues in each of the three MPER-TMD2 helices display an average of 60-100 interactions in total, primarily constituted of residues K683 and W672 (Table 1). These interactions are the consequence of the near-symmetric trimer arrangement and the inward-facing orientation of these residues in the observed MPER-TMD2 conformation. Moreover, residue W680 displays interactions with the surrounding lipid molecules, both with the polar head groups or the acyl chains of the lipids (Fig. 7 and Table 2). As a result, the epitope can be considered inaccessible to incoming antibody molecules. These observations support the experimentally observed deficient antigenicity of MPER-TMD2.

3.3.5 Effect of the flanking lysines on the MPER-TMD1 model

Finally, to determine to what extent factors conditioning accessibility of 10E8 epitope on MPER-TMD1, i.e., loss of symmetry and inter-helical interactions of the MPER-TMD1 trimer, depend on the truncation of the TMD at A700 and/or on the presence of lysine residues at both ends, three additional models were generated: 1) residues 671-700 without lysines (MPER-TMD1$_{no\text{-}lys}$); 2) residues 671-700 with three lysines at the N-terminus (MPER-

$TMD1_N$) and 3) residues 671-700 with three lysines at the C-terminus (MPER-$TMD1_C$). MD simulations were performed for 200 ns, and the last 100 ns were considered for analysis (Figs. 8 and S2, and Tables S1-4).

MPER-$TMD1_{no\text{-}lys}$ resembles most closely the results obtained with the MPER-TMD2 construct devoid of lysines, with a RMSD of 2.6 ± 0.1 Å (Fig. S2A) and an increased verticality of the helices (tilt angles between 7-20°) (Fig. S2C). In contrast, RMSD values are significantly higher for MPER-$TMD1_C$ (3.2 ± 0.3 Å) and especially, for MPER-$TMD1_N$ (4.7 ± 0.2 Å), the latter displaying a similar value to that of the MPER-TMD1 construct flanked by lysines. Similarly, two of the three helices of either N or C lysine-flanked assemblies display a significant increase in their tilt angles. However, unlike MPER-TMD2, inspection of the number of atomic interaction pairs between adjacent helical pairs in MPER-$TMD1_{no\text{-}lys}$ suggests a loss of symmetry in the latter, displaying an extensive contact interface between the CA helices (Fig. S2B), where residue pairs scoring N_P>15 extend the full length of the MPER-TMD1 peptide (Fig. 8). This situation is replicated in MPER-$TMD1_N$, between helices A and B. The similarity of the evolved conformations provides evidence that truncation of the peptide at residue 700, destabilizes the symmetric trimer structure, preferring an assembly whereby two helices are closely associated, with the third attached by hydrophobic residues in the region between I682 and I693. Addition of lysine residues at the C-terminus in MPER-$TMD1_C$ and in the original MPER-TMD1 assembly flanked by lysines, promotes further destabilization of the observed 'dimer' interfaces, with the maximum number of inter-helical interactions capped at 350 (Fig. S2B), and with fewer residue pairs scoring N_P>15 (Fig. 8). These results imply that truncation of the TMD causes a rearrangement of the TMD structure favoring trimer asymmetry and a dimer interface, which is partially inhibited by including lysines after A700.

When scoring interactions with lipids, a similar trend is exhibited for the three new simulations (Tables S1 and S2) and that of MPER-TMD1, regardless of the absence or presence of lysine tags, with W678 or W680 interacting with the phospholipid headgroups of

the upper leaflet in at least one of the monomers in each assembly and, to a lesser extent, with K668 and K670 (MPER-TMD1$_N$, helix B) and W672 or F673 (MPER-TMD1$_C$, A and B helices, respectively). Furthermore, residues that strongly interact with the hydrophobic core of the membrane are conserved in all MPER-TMD1 simulations. Thus, due to the similar degree of insertion into the membrane of all the models, no interactions are recorded between MPER-TMD1$_{no\text{-}lys}$ or MPER-TMD1$_N$ C-terminal residues and the phospholipid headgroups in the lower leaflet, as opposed to constructs bearing lysines at the C-terminus, which display interactions through the lysine residues.

Finally, the average number of atomic interactions of the main epitope residues with adjacent helices (Table S3) and the surrounding lipids (Table S4) was calculated. In MPER-TMD1$_{no\text{-}lys}$ epitope residues in each of the three helices display an average of 60-110 interactions in total, primarily constituted of residues W672 and K683. Moreover, residue W680 displays extensive interactions with the surrounding lipid molecules. These results replicate those obtained for MPER-TMD2 and advocate that truncation to residue 700 alone is insufficient to expose the antibody epitope, despite destabilization of the symmetric trimer arrangement. In MPER-TMD1$_N$, the epitope in helix A can be considered unavailable, with nearly 200 atomic interactions in the region F673 to K683. The 50-recorded interactions for helix B primarily originate from W672. In helix C, only 10 protein interactions are observed from W680 and K683, which also dominate lipid interactions throughout. Similar to the MPER-TMD1 model flanked by lysines at both ends, these results reveal a single helix (C) where the N-terminal epitope residues (N671, W672 and F673) are exposed to solvent, engaging in minimal protein (1) and lipid (32) and might effectively interact with the antibody. Finally, in MPER-TMD$_C$, helix B displays the minimum number of protein (14) and lipid (42) interactions with such residues. These results suggest the addition of lysine residues to the N-terminus is an effective strategy for epitope exposure.

4- Discussion

In the present work, we have analyzed the effect of HIV-1 gp41 TM domain on the exposure of the MPER epitope at the surface of lipid bilayers. With this aim, we designed two MPER-TMD sequences based on previously reported mutagenesis studies of the TMD [9]: MPER-TMD1, in which the TMD was truncated at A700, and MPER-TMD2, which spans the full TMD up to R709 (Fig. 1). Given the critical role of the lipid membrane in various stages of the HIV virus cycle [56] and particularly, in the recognition of their epitopes by the antibodies 4E10 and 10E8 [30, 48, 57], it has been argued that not only Env structure but also its membrane environment should be preserved in the development of vaccines that aim to elicit anti-MPER antibodies targeting its C-terminal region (i.e., 4E10/10E8) [19, 58]. Therefore, MPER-TMD1 and MPER-TMD2 were formulated in HIV-1 like cholesterol-enriched liposomal-vaccines [33] and immunochemical assays were performed to test the antigenicity of both candidates. The results revealed that MPER-TMD1, but not MPER-TMD2, was capable of specific and efficient antibody recognition by anti-MPER bnAbs (Figs. 2, 3 and S1). Moreover, MPER-TMD1 was shown to migrate as dimers under denaturing conditions. Consistent with this behavior, reported mutagenesis studies of the TMD showed that truncation of residues 705 to 716 induced partial destabilization of the trimer [13]. Moreover, analyses of the NMR spectra of a gp41 construct terminating at residue 705 showed conformational flexibility in the CHR-MPER-TM region of gp41, pointing to the potential of this region to display conformations other than a stable trimer during the fusion process [59]. In contrast, our experimental data indicated that the longer MPER-TMD2 was reportedly more stable, demonstrated by the presence of dimers and trimers following denaturing treatment (Figs. 2, 3 and S1). This assorted dimer and trimer migration pattern was also reported for a similar peptide containing the full-length MPER (residues 661-708 plus four C-terminal lysines) incorporated into DMPC nanodiscs [29]. These results suggest that the TM domain is instrumental in the trimerization process, whereas the MPER domain does not play a significant role. However, opposing our results, high affinity recognition of

bnAb 4E10 to that peptide was reported [29]. Besides N-terminal elongation and C-terminal addition of lysines, the physical and chemical properties of the selected lipids utilized in both studies were also dissimilar. The thickness of a DMPC bilayer is reported to be of around 35-37 Å [60, 61], significantly thinner than that of cholesterol-enriched phospholipid bilayers [61] such as the viral envelope [33, 62]. Cholesterol augments membrane physical properties such as rigidity and thickness, thereby affecting TMD helix accommodation within the lipid bilayer [63], and conceivably, modulating the MPER-scaffolding capacity, i.e., the antigenicity of the MPER-TMD constructs. This might account for the reported differences observed between the two studies and highlights the importance of the membrane composition in the design of liposomal vaccines targeting the 10E8 epitope.

The computational analysis of the candidate liposomal vaccines confirms the above experimental observations and reveals the molecular mechanism underlying efficient epitope exposure in the MPER-TMD1 scaffold. Overall, two distinctive conformations of the MPER-TMD assemblies were observed. Whereas MPER-TMD2 closely resembles the three-fold assembly observed in the NMR structure of the HIV-1 TMD [13], the close association of the transmembrane helices is noticeably perturbed in all MPER-TMD1-based models resulting in an asymmetric assembly (Figs. 4-6, 8 and S2). Therefore, destabilization of the MPER-TMD1 trimer, can be attributed to truncation of the TMD following A700 to some extent. It should be emphasized that the residues involved in inter-helical interactions in the MPER-TMD2 trimer are all present in MPER-TMD1 assemblies; thus, it is primarily environmental interactions that influence the dynamics of the MPER-TMD derived scaffolds. Substantial interactions between V701 and L702 and the acyl tails, and between R709 and the phospholipid head groups, observed in MPER-TMD2 (Fig. 7) are lost upon truncation; thus, the observed reorientation of the helices to an asymmetric arrangement in MPER-TMD1-based assemblies can be attributed to the absence of lipid interactions with such residues. We speculate that, as previously demonstrated [9], R709 is particularly crucial for membrane anchoring, as truncation of the region following this residue results in a stable assembly, profoundly similar to the initial construct. In addition, the resulting conformation of MPER-

TMD1 trimers bearing lysines accommodates for the positively charged lysine residues, which are predominantly excluded from the membrane hydrophobic core contributing to the perturbed conformation of the MPER-TMD1 trimer, the underlying α-helices and the bilayer. These effects were not detected in the MPER-TMD2 simulation, in which sequence composition, length and tilt angles are more compatible with the hydrophobic core dimensions of this bilayer. Moreover, MPER-TMD1 models devoid of lysines or with lysines at the N-terminus reveal a prominent new dimer interface indicating that TMD helices have the potential to adopt multiple conformations. It is tempting to speculate that in the context of the whole protein and due to the dynamic nature of Env [4, 64, 65] the TMD might suffer conformational changes, such as reorientations, variations in the tilt angles or dissociation events, which might perturb the viral envelope priming it for fusion with the cellular membrane, or alternatively, which might permit establishing interactions with TMD helices from adjacent trimers at crucial moments of the fusion cycle.

The specific molecular interactions of the residues within the epitope region might be used to rationalize the distinct antigenicity pattern of the MPER-TMD scaffolds (Tables 1, 2, and S1 and S2). Main epitope residues in MPER-TMD2 and in MPER-TMD1$_{no\text{-}lys}$ face the core of the trimer with crucial residues W672 and K683 engaged in inter-helix contacts and with W680 interacting with the lipid molecules. Although residue W680 is not essential for the binding of 4E10 and 10E8 to their epitopes in solution it is important for the viral-neutralization function of these antibodies [24, 66-68]. Moreover, it was shown to modulate the immunogenicity of MPER-derived peptides by shifting the specificity of the immune response towards the N-terminus when W680 was embedded in the membrane [69]. Thus, in both models, the MPER epitope faces the interior of the trimer in a conformation that might hinder antibody recognition at membrane surfaces. These observations might have implications regarding the structure of the TMD in the context of the pre-fusion conformation of the native Env. Since the conformation of the MPER-TMD2 scaffold greatly resembles the original structure solved by NMR in bicelles [13], we hypothesize that such structure would not represent the neutralization competent structure recognized by 10E8. Consequently, the NMR structure is

also likely to differ from the pre-fusion structure of the native Env which was recently solved by cryo-EM bound to two molecules of bnAb 10E8 [4]. In the case of the MPER-TMD1 construct flanked by lysines, epitope residues within each helix display a distinct interaction pattern. Epitope residues in helix B are not engaged in inter-helix interactions in helix B but are buried in the membrane, and thus, inaccessible to the antibodies. In contrast, epitope residues in helices A and C were not found to interact with lipids. However, similarly to MPER-TMD2, W672 and K683 in helix A are engaged in inter-helix interactions possibly precluding antibody recognition of the epitope. Finally, although C-terminal epitope residues W680 and K683 are interacting with residues in other helices, N-terminal epitope residues N671, W672 and F673 are fully exposed. A similar pattern is recorded for helix C in MPER-TMD1$_N$. Although both protein and lipid molecules will likely be perturbed to some extent by approach of the antibody, the data presented herein provide evidence that the epitope region undergoes conformational differences depending on the protein scaffold used to present the epitope, being considerably more likely that the antibody will recognize MPER-TMD1 or MPER-TMD1$_N$ than MPER-TMD2, MPER-TMD1$_{no\text{-}lys}$ or MPER-TMD1$_C$, where the epitope is either stably embedded in the trimer core or interacting with lipid molecules. We hypothesize that antibody recognition of the exposed epitope and subsequent binding to these peptides would require a two-step binding mechanism, in which the antibody would first approach the MPER and bind to the N-terminal residues. This interaction would conceivably alter the pre-existing inter-helix interactions at the C-terminal part of the epitope and the rest of the paratope could then be effectively accommodated.

Overall, these results suggest that inclusion of particular attributes that destabilize the trimer, i.e., truncation of the TMD, and expose the epitope, i.e., addition of N-terminal lysines, would likely aid the optimization of MPER-TMD derived peptides in the context of vaccine design. In the context of the virus, the intrinsic dynamics of Env [4] might transiently extract and expose the MPER leading to the engagement of B-cell receptors, but in the absence of these forces, in the context of a minimal immunogen, MPER should be readily exposed to the immune system. In this regard, extensive mutagenesis studies, performed by Dev *et al.*,

examining the antigenic structure of the Env ectodomain [13] showed that even the most simple mutations in the TMD region (F685A, I686A, G690A, L692A, G694V, L695A, I697A) modulated the antigenic surface of Env and specifically, increased viral sensitivity to 10E8. Residues, F685, I686, L692 and I697 are involved in crucial inter-helical interactions in the MPER-TMD2 trimer only, thus it can be inferred that mutation of these residues might destabilize the canonical structure, and potentially lead to the exposure of expose the 10E8 epitope.

All in all, the immunochemical assays and in-depth MD analyses reported herein suggest that the structure-based design of effective liposomal vaccines based on the MPER-TMD might require a rational mutation strategy of the TMD along with a systematic analysis of the lipid bilayer, to achieve efficient exposure of the MPER epitope at the membrane surface. Overall, this study advances our understanding of the requirements that must be met by a liposome-based peptide-vaccine targeting this critical antigenic site on Env.

ACKNOWLEDGMENTS

Computational resources were awarded through RES in Magerit based in Spain at CeSViMa – Universidad Politécnica de Madrid. We thank RES for providing computational resources and technical support. We acknowledge the financial support of the Spanish Government (MINECO Grant BIO2015-64421-R) and the Basque Government (Grant IT838-13). BA was recipient of a post-graduate Grant (ESPDOC2015) from the University of the Basque Country (UPV/EHU), VO was supported by a CASE studentship funded by BBSRC and Pfizer Neusentis and E.R. was recipient of a predoctoral fellowship (PRE_2014_2_264) from the Basque Government.

Author contributions: J.L.N, B.A., and CD conceived the research and designed the experiments; V.O. performed and analized the MD simulations. J.T. and B.A. performed and analyzed biophysical and immunochemical characterizations; E.R. produced the Fabs. V.O., C.D. and B.A. wrote the paper; all authors critically revised the manuscript and all authors approved it. The authors thank Dr. Sánchez-Eugenia for valuable discussions and technical advice.

REFERENCES:

[1] D. Lyumkis, J.P. Julien, N. de Val, A. Cupo, C.S. Potter, P.J. Klasse, D.R. Burton, R.W. Sanders, J.P. Moore, B. Carragher, I.A. Wilson, A.B. Ward, Cryo-EM structure of a fully glycosylated soluble cleaved HIV-1 envelope trimer, Science, 342 (2013) 1484-1490. http://dx.doi.org/10.1126/science.1245627

[2] J.P. Julien, A. Cupo, D. Sok, R.L. Stanfield, D. Lyumkis, M.C. Deller, P.J. Klasse, D.R. Burton, R.W. Sanders, J.P. Moore, A.B. Ward, I.A. Wilson, Crystal structure of a soluble cleaved HIV-1 envelope trimer, Science, 342 (2013) 1477-1483. http://dx.doi.org/10.1126/science.1245625

[3] M. Pancera, T. Zhou, A. Druz, I.S. Georgiev, C. Soto, J. Gorman, J. Huang, P. Acharya, G.Y. Chuang, G. Ofek, G.B. Stewart-Jones, J. Stuckey, R.T. Bailer, M.G. Joyce, M.K. Louder, N. Tumba, Y. Yang, B. Zhang, M.S. Cohen, B.F. Haynes, J.R. Mascola, L. Morris, J.B. Munro, S.C. Blanchard, W. Mothes, M. Connors, P.D. Kwong, Structure and immune recognition of trimeric pre-fusion HIV-1 Env, Nature, 514 (2014) 455-461. http://dx.doi.org/10.1038/nature13808

[4] J.H. Lee, G. Ozorowski, A.B. Ward, Cryo-EM structure of a native, fully glycosylated, cleaved HIV-1 envelope trimer, Science, 351 (2016) 1043-1048. http://dx.doi.org/10.1126/science.aad2450

[5] G. Ozorowski, J. Pallesen, N. de Val, D. Lyumkis, C.A. Cottrell, J.L. Torres, J. Copps, R.L. Stanfield, A. Cupo, P. Pugach, J.P. Moore, I.A. Wilson, A.B. Ward, Open and closed structures reveal allostery and pliability in the HIV-1 envelope spike, Nature, 547 (2017) 360–363. http://dx.doi.org/10.1038/nature23010

[6] A.B. Ward, I.A. Wilson, The HIV-1 envelope glycoprotein structure: nailing down a moving target, Immunol Rev, 275 (2017) 21-32. http://dx.doi.org/10.1111/imr.12507

[7] J.W. Dubay, S.J. Roberts, B.H. Hahn, E. Hunter, Truncation of the human immunodeficiency virus type 1 transmembrane glycoprotein cytoplasmic domain blocks virus infectivity, J Virol, 66 (1992) 6616-6625.

[8] D. Gabuzda, U. Olshevsky, P. Bertani, W.A. Haseltine, J. Sodroski, Identification of membrane anchorage domains of the HIV-1 gp160 envelope glycoprotein precursor, J Acquir Immune Defic Syndr, 4 (1991) 34-40. http://dx.doi.org/10.1097/00126334-199101000-00005

[9] L. Yue, L. Shang, E. Hunter, Truncation of the Membrane-Spanning Domain of Human Immunodeficiency Virus Type 1 Envelope Glycoprotein Defines Elements Required for Fusion, Incorporation, and Infectivity, J. Virol., 83 (2009) 11588-11598. http://dx.doi.org/10.1128/jvi.00914-09

[10] L. Shang, L. Yue, E. Hunter, Role of the membrane-spanning domain of human immunodeficiency virus type 1 envelope glycoprotein in cell-cell fusion and virus infection, J Virol, 82 (2008) 5417-5428. http://dx.doi.org/10.1128/JVI.02666-07

[11] R.J. Owens, C. Burke, J.K. Rose, Mutations in the membrane-spanning domain of the human immunodeficiency virus envelope glycoprotein that affect fusion activity, J Virol, 68 (1994) 570-574.

[12] B. Apellaniz, J.L. Nieva, Fusion-competent state induced by a C-terminal HIV-1 fusion peptide in cholesterol-rich membranes, Biochim Biophys Acta, 1848 (2015) 1014-1022. http://dx.doi.org/10.1016/j.bbamem.2015.01.011

[13] J. Dev, D. Park, Q. Fu, J. Chen, H.J. Ha, F. Ghantous, T. Herrmann, W. Chang, Z. Liu, G. Frey, M.S. Seaman, B. Chen, J.J. Chou, Structural basis for membrane anchoring of HIV-1 envelope spike, Science, 353 (2016) 172-175. http://dx.doi.org/10.1126/science.aaf7066

[14] K. Miyauchi, J. Komano, Y. Yokomaku, W. Sugiura, N. Yamamoto, Z. Matsuda, Role of the specific amino acid sequence of the membrane-spanning domain of human immunodeficiency virus type 1 in membrane fusion, J Virol, 79 (2005) 4720-4729. http://dx.doi.org/10.1128/JVI.79.8.4720-4729.2005

[15] A. Ashkenazi, O. Faingold, Y. Shai, HIV-1 fusion protein exerts complex immunosuppressive effects, Trends in biochemical sciences, 38 (2013) 345-349. http://dx.doi.org/10.1016/j.tibs.2013.04.003

[16] E. Rotem, E.M. Reuven, Y.A. Klug, Y. Shai, The Transmembrane Domain of HIV-1 gp41 Inhibits T-Cell Activation by Targeting Multiple T-Cell Receptor Complex Components through Its GxxxG Motif, Biochemistry, 55 (2016) 1049-1057. http://dx.doi.org/10.1021/acs.biochem.5b01307

[17] E.M. Reuven, M. Ali, E. Rotem, R. Schwarzter, A. Gramatica, A.H. Futerman, Y. Shai, The HIV-1 envelope transmembrane domain binds TLR2 through a distinct dimerization motif and inhibits TLR2-mediated responses, PLoS Pathog, 10 (2014) e1004248. http://dx.doi.org/10.1371/journal.ppat.1004248

[18] Y.A. Klug, E. Rotem, R. Schwarzer, Y. Shai, Mapping out the intricate relationship of the HIV envelope protein and the membrane environment, Biochim Biophys Acta, 1859 (2017) 550-560. http://dx.doi.org/10.1016/j.bbamem.2016.10.012

[19] B. Apellaniz, J.L. Nieva, The Use of Liposomes to Shape Epitope Structure and Modulate Immunogenic Responses of Peptide Vaccines Against HIV MPER, Advances in protein chemistry and structural biology, 99 (2015) 15-54. http://dx.doi.org/10.1016/bs.apcsb.2015.03.002

[20] M. Montero, N.E. van Houten, X. Wang, J.K. Scott, The membrane-proximal external region of the human immunodeficiency virus type 1 envelope: dominant site of antibody neutralization and target for vaccine design, Microbiol Mol Biol Rev, 72 (2008) 54-84. http://dx.doi.org/10.1128/MMBR.00020-07

[21] L.E. McCoy, D.R. Burton, Identification and specificity of broadly neutralizing antibodies against HIV, Immunol Rev, 275 (2017) 11-20. http://dx.doi.org/10.1111/imr.12484

[22] N. Cerutti, J.L. Loredo-Varela, C. Caillat, W. Weissenhorn, Antigp41 membrane proximal external region antibodies and the art of using the membrane for neutralization, Curr Opin HIV AIDS, 12 (2017) 250-256. http://dx.doi.org/10.1097/COH.0000000000000364

[23] G. Stiegler, R. Kunert, M. Purtscher, S. Wolbank, R. Voglauer, F. Steindl, H. Katinger, A potent cross-clade neutralizing human monoclonal antibody against a novel epitope on gp41 of human immunodeficiency virus type 1, AIDS Res Hum Retroviruses, 17 (2001) 1757-1765. http://dx.doi.org/10.1089/08892220152741450

[24] J. Huang, G. Ofek, L. Laub, M.K. Louder, N.A. Doria-Rose, N.S. Longo, H. Imamichi, R.T. Bailer, B. Chakrabarti, S.K. Sharma, S.M. Alam, T. Wang, Y. Yang, B. Zhang, S.A. Migueles, R. Wyatt, B.F. Haynes, P.D. Kwong, J.R. Mascola, M. Connors, Broad and potent

neutralization of HIV-1 by a gp41-specific human antibody, Nature, 491 (2012) 406-412. http://dx.doi.org/10.1038/nature11544

[25] A. Irimia, A.M. Serra, A. Sarkar, R. Jacak, O. Kalyuzhniy, D. Sok, K.L. Saye-Francisco, T. Schiffner, R. Tingle, M. Kubitz, Y. Adachi, R.L. Stanfield, M.C. Deller, D.R. Burton, W.R. Schief, I.A. Wilson, Lipid interactions and angle of approach to the HIV-1 viral membrane of broadly neutralizing antibody 10E8: Insights for vaccine and therapeutic design, PLoS Pathog, 13 (2017) e1006212. http://dx.doi.org/10.1371/journal.ppat.1006212

[26] M. Montero, N. Gulzar, K.A. Klaric, J.E. Donald, C. Lepik, S. Wu, S. Tsai, J.P. Julien, A.J. Hessell, S. Wang, S. Lu, D.R. Burton, E.F. Pai, W.F. Degrado, J.K. Scott, Neutralizing epitopes in the membrane-proximal external region of HIV-1 gp41 are influenced by the transmembrane domain and the plasma membrane, J Virol, 86 (2012) 2930-2941. http://dx.doi.org/10.1128/JVI.06349-11

[27] B. Apellaniz, E. Rujas, P. Carravilla, J. Requejo-Isidro, N. Huarte, C. Domene, J.L. Nieva, Cholesterol-Dependent Membrane Fusion Induced by the gp41 Membrane-Proximal External Region-Transmembrane Domain Connection Suggests a Mechanism for Broad HIV-1 Neutralization, J Virol, 88 (2014) 13367-13377. http://dx.doi.org/10.1128/JVI.02151-14

[28] B. Apellaniz, E. Rujas, S. Serrano, K. Morante, K. Tsumoto, J.M. Caaveiro, M.A. Jimenez, J.L. Nieva, The Atomic Structure of the HIV-1 gp41 Transmembrane Domain and Its Connection to the Immunogenic Membrane-proximal External Region, J Biol Chem, 290 (2015) 12999-13015. http://dx.doi.org/10.1074/jbc.M115.644351

[29] T.M. Reichart, M.M. Baksh, J.K. Rhee, J.D. Fiedler, S.G. Sligar, M.G. Finn, M.B. Zwick, P.E. Dawson, Trimerization of the HIV Transmembrane Domain in Lipid Bilayers

Modulates Broadly Neutralizing Antibody Binding, Angew Chem Int Ed Engl, 55 (2016) 2688-2692. http://dx.doi.org/10.1002/anie.201508421

[30] E. Rujas, J.M. Caaveiro, A. Partida-Hanon, N. Gulzar, K. Morante, B. Apellaniz, M. Garcia-Porras, M. Bruix, K. Tsumoto, J.K. Scott, M.A. Jimenez, J.L. Nieva, Structural basis for broad neutralization of HIV-1 through the molecular recognition of 10E8 helical epitope at the membrane interface, Sci Rep, 6 (2016) 38177. http://dx.doi.org/10.1038/srep38177

[31] Z.Y. Sun, K.J. Oh, M. Kim, J. Yu, V. Brusic, L. Song, Z. Qiao, J.H. Wang, G. Wagner, E.L. Reinherz, HIV-1 broadly neutralizing antibody extracts its epitope from a kinked gp41 ectodomain region on the viral membrane, Immunity, 28 (2008) 52-63. http://dx.doi.org/10.1016/j.immuni.2007.11.018

[32] N. Huarte, M. Lorizate, R. Maeso, R. Kunert, R. Arranz, J.M. Valpuesta, J.L. Nieva, The broadly neutralizing anti-human immunodeficiency virus type 1 4E10 monoclonal antibody is better adapted to membrane-bound epitope recognition and blocking than 2F5, J Virol, 82 (2008) 8986-8996. http://dx.doi.org/10.1128/JVI.00846-08

[33] B. Brugger, B. Glass, P. Haberkant, I. Leibrecht, F.T. Wieland, H.G. Krausslich, The HIV lipidome: a raft with an unusual composition, Proc Natl Acad Sci U S A, 103 (2006) 2641-2646. http://dx.doi.org/10.1073/pnas.0511136103

[34] J.A. Yethon, R.F. Epand, B. Leber, R.M. Epand, D.W. Andrews, Interaction with a membrane surface triggers a reversible conformational change in Bax normally associated with induction of apoptosis, J Biol Chem, 278 (2003) 48935-48941. http://dx.doi.org/10.1074/jbc.M306289200

[35] S. Jo, T. Kim, V.G. Iyer, W. Im, CHARMM-GUI: a web-based graphical user interface for CHARMM, J Comput Chem, 29 (2008) 1859-1865. http://dx.doi.org/10.1002/jcc.20945

[36] S. Jo, J.B. Lim, J.B. Klauda, W. Im, CHARMM-GUI Membrane Builder for mixed bilayers and its application to yeast membranes, Biophys J, 97 (2009) 50-58. http://dx.doi.org/10.1016/j.bpj.2009.04.013

[37] E.L. Wu, X. Cheng, S. Jo, H. Rui, K.C. Song, E.M. Davila-Contreras, Y. Qi, J. Lee, V. Monje-Galvan, R.M. Venable, J.B. Klauda, W. Im, CHARMM-GUI Membrane Builder toward realistic biological membrane simulations, J Comput Chem, 35 (2014) 1997-2004. http://dx.doi.org/10.1002/jcc.23702

[38] J.C. Phillips, R. Braun, W. Wang, J. Gumbart, E. Tajkhorshid, E. Villa, C. Chipot, R.D. Skeel, L. Kale, K. Schulten, Scalable molecular dynamics with NAMD, J Comput Chem, 26 (2005) 1781-1802. http://dx.doi.org/10.1002/jcc.20289

[39] J.B. Klauda, R.M. Venable, J.A. Freites, J.W. O'Connor, D.J. Tobias, C. Mondragon-Ramirez, I. Vorobyov, A.D. MacKerell, Jr., R.W. Pastor, Update of the CHARMM all-atom additive force field for lipids: validation on six lipid types, J Phys Chem B, 114 (2010) 7830-7843. http://dx.doi.org/10.1021/jp101759q

[40] W.L. Jorgensen, J. Chandrasekhar, J.D. Madura, R.W. Impey, M.L. Klein, Comparison of simple potential functions for simulating liquid water, J Chem Phys, 79 (1983) 926-935. http://dx.doi.org/10.1063/1.445869

[41] D. Beglov, B. Roux, Finite representation of an infinite bulk system: Solvent boundary potential for computer simulations, J Chem Phys, 100 (1994) 9050-9063. http://dx.doi.org/10.1063/1.466711

[42] T. Darden, D. York, L. Pedersen, Particle mesh Ewald: An N· log(N) method for Ewald sums in large systems, J Chem Phys, 98 (1993) 10089-10092. http://dx.doi.org/10.1063/1.464397

[43] L. Verlet, Computer "Experiments" on Classical Fluids. I. Thermodynamical Properties of Lennard-Jones Molecules, Phys. Rev., 159 (1967) 98-103.

[44] S. Miyamoto, P.A. Kollman, SETTLE: an analytical version of the SHAKE and RATTLE algorithm for rigid water models, J. Comput. Chem., 13 (1992) 952-962. http://dx.doi.org/10.1002/jcc.540130805

[45] S.E. Feller, Y. Zhang, R.W. Pastor, B.R. Brooks, Constant pressure molecular dynamics simulation: The Langevin piston method, J Chem Phys, 103 (1995) 4613-4621. http://dx.doi.org/10.1063/1.470648

[46] G.J. Martyna, D.J. Tobias, M.L. Klein, Constant pressure molecular dynamics algorithms, J Chem Phys, 101 (1994) 4177-4189. http://dx.doi.org/10.1063/1.467468

[47] W. Humphrey, A. Dalke, K. Schulten, VMD: Visual molecular dynamics, J Mol Graphics, 14 (1996) 33-38. http://dx.doi.org/10.1016/0263-7855(96)00018-5

[48] E. Rujas, S. Insausti, M. Garcia-Porras, R. Sanchez-Eugenia, K. Tsumoto, J.L. Nieva, J.M. Caaveiro, Functional Contacts between MPER and the Anti-HIV-1 Broadly Neutralizing Antibody 4E10 Extend into the Core of the Membrane, J Mol Biol, 429 (2017) 1213-1226. http://dx.doi.org/10.1016/j.jmb.2017.03.008

[49] E. Rujas, N. Gulzar, K. Morante, K. Tsumoto, J.K. Scott, J.L. Nieva, J.M. Caaveiro, Structural and Thermodynamic Basis of Epitope Binding by Neutralizing and Nonneutralizing Forms of the Anti-HIV-1 Antibody 4E10, J Virol, 89 (2015) 11975-11989. http://dx.doi.org/10.1128/JVI.01793-15

[50] O.K. Haffar, D.J. Dowbenko, P.W. Berman, Topogenic analysis of the human immunodeficiency virus type 1 envelope glycoprotein, gp160, in microsomal membranes, J Cell Biol, 107 (1988) 1677-1687. http://dx.doi.org/10.1083/jcb.107.5.1677

[51] F.M. Brunel, M.B. Zwick, R.M. Cardoso, J.D. Nelson, I.A. Wilson, D.R. Burton, P.E. Dawson, Structure-function analysis of the epitope for 4E10, a broadly neutralizing human immunodeficiency virus type 1 antibody, J Virol, 80 (2006) 1680-1687. http://dx.doi.org/10.1128/JVI.80.4.1680-1687.2006

[52] R. Abe, J.M. Caaveiro, H. Kozuka-Hata, M. Oyama, K. Tsumoto, Mapping ultra-weak protein-protein interactions between heme transporters of Staphylococcus aureus, J Biol Chem, 287 (2012) 16477-16487. http://dx.doi.org/10.1074/jbc.M112.346700

[53] T.S. Young, I. Ahmad, J.A. Yin, P.G. Schultz, An enhanced system for unnatural amino acid mutagenesis in E. coli, J Mol Biol, 395 (2010) 361-374. http://dx.doi.org/10.1016/j.jmb.2009.10.030

[54] S.H. White, Translocons, thermodynamics, and the folding of membrane proteins, FEBS Lett, 555 (2003) 116-121.

[55] B. Apellaniz, S. Nir, J.L. Nieva, Distinct mechanisms of lipid bilayer perturbation induced by peptides derived from the membrane-proximal external region of HIV-1 gp41, Biochemistry, 48 (2009) 5320-5331. 10.1021/bi900504t

[56] E.O. Freed, HIV-1 assembly, release and maturation, Nat Rev Microbiol, 13 (2015) 484-496. http://dx.doi.org/10.1038/nrmicro3490

[57] E. Rujas, J.M. Caaveiro, S. Insausti, M. Garcia-Porras, K. Tsumoto, J.L. Nieva, Peripheral Membrane Interactions Boost the Engagement by an Anti-HIV-1 Broadly Neutralizing Antibody, J Biol Chem, 292 (2017) 5571-5583. http://dx.doi.org/10.1074/jbc.M117.775429

[58] A. Irimia, A. Sarkar, R.L. Stanfield, I.A. Wilson, Crystallographic Identification of Lipid as an Integral Component of the Epitope of HIV Broadly Neutralizing Antibody 4E10, Immunity, 44 (2016) 21-31. http://dx.doi.org/10.1016/j.immuni.2015.12.001

[59] N.A. Lakomek, J.D. Kaufman, S.J. Stahl, J.M. Louis, A. Grishaev, P.T. Wingfield, A. Bax, Internal dynamics of the homotrimeric HIV-1 viral coat protein gp41 on multiple time scales, Angew Chem Int Ed Engl, 52 (2013) 3911-3915. http://dx.doi.org/10.1002/anie.201207266

[60] N. Kucerka, M.P. Nieh, J. Katsaras, Fluid phase lipid areas and bilayer thicknesses of commonly used phosphatidylcholines as a function of temperature, Biochim Biophys Acta, 1808 (2011) 2761-2771. http://dx.doi.org/10.1016/j.bbamem.2011.07.022

[61] J. Pan, T.T. Mills, S. Tristram-Nagle, J.F. Nagle, Cholesterol perturbs lipid bilayers nonuniversally, Phys Rev Lett, 100 (2008) 198103. http://dx.doi.org/10.1103/PhysRevLett.100.198103

[62] N. Huarte, P. Carravilla, A. Cruz, M. Lorizate, J.A. Nieto-Garai, H.G. Krausslich, J. Perez-Gil, J. Requejo-Isidro, J.L. Nieva, Functional organization of the HIV lipid envelope, Sci Rep, 6 (2016) 34190. http://dx.doi.org/10.1038/srep34190

[63] T.J. McIntosh, S.A. Simon, Bilayers as protein solvents: role of bilayer structure and elastic properties, J Gen Physiol, 130 (2007) 225-227. http://dx.doi.org/10.1085/jgp.200709841

[64] J.B. Munro, J. Gorman, X. Ma, Z. Zhou, J. Arthos, D.R. Burton, W.C. Koff, J.R. Courter, A.B. Smith, 3rd, P.D. Kwong, S.C. Blanchard, W. Mothes, Conformational dynamics of single HIV-1 envelope trimers on the surface of native virions, Science, 346 (2014) 759-763. http://dx.doi.org/10.1126/science.1254426

[65] J.B. Munro, W. Mothes, Structure and Dynamics of the Native HIV-1 Env Trimer, J Virol, 89 (2015) 5752-5755. http://dx.doi.org/10.1128/JVI.03187-14

[66] M.B. Zwick, R. Jensen, S. Church, M. Wang, G. Stiegler, R. Kunert, H. Katinger, D.R. Burton, Anti-human immunodeficiency virus type 1 (HIV-1) antibodies 2F5 and 4E10 require surprisingly few crucial residues in the membrane-proximal external region of glycoprotein gp41 to neutralize HIV-1, J Virol, 79 (2005) 1252-1261. http://dx.doi.org/10.1128/JVI.79.2.1252-1261.2005

[67] T. Bradley, A. Trama, N. Tumba, E. Gray, X. Lu, N. Madani, F. Jahanbakhsh, A. Eaton, S.M. Xia, R. Parks, K.E. Lloyd, L.L. Sutherland, R.M. Scearce, C.M. Bowman, S. Barnett,

S.S. Abdool-Karim, S.D. Boyd, B. Melillo, A.B. Smith, 3rd, J. Sodroski, T.B. Kepler, S.M. Alam, F. Gao, M. Bonsignori, H.X. Liao, M.A. Moody, D. Montefiori, S. Santra, L. Morris, B.F. Haynes, Amino Acid Changes in the HIV-1 gp41 Membrane Proximal Region Control Virus Neutralization Sensitivity, EBioMedicine, 12 (2016) 196-207. http://dx.doi.org/10.1016/j.ebiom.2016.08.045

[68] K.J. Nakamura, J.S. Gach, L. Jones, K. Semrau, J. Walter, F. Bibollet-Ruche, J.M. Decker, L. Heath, W.D. Decker, M. Sinkala, C. Kankasa, D. Thea, J. Mullins, L. Kuhn, M.B. Zwick, G.M. Aldrovandi, 4E10-resistant HIV-1 isolated from four subjects with rare membrane-proximal external region polymorphisms, PLoS One, 5 (2010) e9786. http://dx.doi.org/10.1371/journal.pone.0009786

[69] M. Kim, L. Song, J. Moon, Z.Y. Sun, A. Bershteyn, M. Hanson, D. Cain, S. Goka, G. Kelsoe, G. Wagner, D. Irvine, E.L. Reinherz, Immunogenicity of membrane-bound HIV-1 gp41 membrane-proximal external region (MPER) segments is dominated by residue accessibility and modulated by stereochemistry, J Biol Chem, 288 (2013) 31888-31901. http://dx.doi.org/10.1074/jbc.M113.494609

Figure Captions:

Figure 1. Description and structure of the HIV-1 gp41 MPER-TMD sequences used in the present study. A) Weblogo representation of MPER-TMD sequence variability of all HIV-1/SIVcpz subtype genomes (filtered web, 5132 sequences) available at the LANL HIV Sequence Database (http://www.hiv.lanl.gov/content/sequence/NEWALIGN/align.html). Gp41 amino acids 671 to 709 are shown (HXBc2 prototypic isolate numbering) color-coded according to their chemical properties (polar - green, neutral - purple, basic - blue, acidic - red and hydrophobic - black) and lines below the logo span the sequences covered by the peptides used in this study. Lines above the logo depict the MPER, N-TMD and C-TMD domains of gp41, and the full epitope of 10E8 antibody is highlighted. The gp41 ectodomain (PDB ID: 5FUU) is shown as ribbons (dark grey). B) Secondary structure of MPER-TM domain derived synthetic peptides. Circular dichroism spectra of MPER-TMD1 and MPER-TMD2 peptides in the low polarity medium provided by 25 % HFIP (left and right panels, respectively).

Figure 2: Association of 10E8 Fab and its mutant version to MPER-TMD1 and MPER-TMD2 reconstituted into cholesterol-enriched vesicles proved by ultracentrifugation in a sucrose gradient. POPC:Chol:PA 10:11:1 (mol:mol) liposomes containing 0.5 % of Rho-PE were reconstituted without peptide (A) or with 30 μM MPER-TMD1 (B) or MPER-TMD2 (C) at a 1:50 peptide-to-lipid molar ratio and were incubated for 15 min at RT and under constant stirring (800 rpm) with 0.07 mg/mL of 10E8 or 10E8 W100bD Fabs (from left to right). The samples were then subjected to ultracentrifugation in a sucrose gradient and harvested in 5 fractions. Peptides (10 kDa bands) and bound or unbound Fabs (25 kDa bands) were size-separated by tricine-PAGE-SDS and proved by Western blot. Effective flotation of the vesicles was monitored following the fluorescence emission of the rhodamine probe included in the liposomes as depicted by the spectra below each panel.

Figure 3. Specific binding of 10E8 Fab to MPER-TMD1 and MPER-TMD2 reconstituted into cholesterol-enriched vesicles or in solution proved by photo-cross-linking. 0.07 mg/mL of 10E8 W100b$_{HC}$*p*BPA Fab was incubated alone, with the peptides in solution or with the peptides reconstituted into membranes, for 15 min at RT and under constant stirring (800 rpm), followed by irradiation with UV-light or no treatment. Peptides, heavy and light chains of the Fabs, and photo-cross-linked Fab-peptide adducts were detected by Coomassie-blue staining. Pink bands at the bottom of the gel revealed the presence of

Rhodamine-labeled liposomes in the samples. The arrow points to the position of the photo-cross-linked product.

Figure 4: Overview of the MPER-TM domain simulations. Snapshots of the MD simulations of MPER-TMD1 (left) and MPER-TMD2 (right) models (A) at time 0 ns (side view) and (B) at time 200 ns (side and top views). The structural models were constructed with UCSF Chimera using 5GHW and 5JNY structures deposited in the PDB. Helices A, B and C are colored in purple, pink and orange, respectively. Main 10E8 epitope residues (^{671}NWF--T---W--K^{683}) are colored lighter in each helix and K683 of one monomer is shown as spheres to mark the predicted starting point for the TMD. The arrows depict the average thickness of the bilayer, which was calculated as the distance between the projected mass distribution of the phosphorous atoms in the upper and lower leaflets, using the MEMPPLUGIN of VMD.

Figure 5: Overall stability of the MPER-TM domain simulations. A) RMSD of the MPER-TM domain residues 671 to 690 in the MPER-TMD1 (red) and MPER-TMD2 (green) models over the course of the simulations. B) Average number of interaction pairs between subunit pairs in the MPER-TMD1 (red), MPER-TMD2 (green) and the initial situation (yellow outline) averaged from frames at 50 ps intervals. An interaction pair is counted if the distance between two atoms is less than 4 Å. C) Tilt angle (τ) of individual helices (residues 671 to 690) with respect to the bilayer normal over the course of the simulations. Each helix is displayed in a different color (A-C helices, purple, pink and orange, respectively). The inset data represent the average tilt angle of each individual helix during the final 100 ns of the simulation.

Figure 6. Inter-helix interactions between protein residues in the MPER-TMD simulations. A) Number of interaction pairs between specific residues in the MPER-TMD1 simulation averaged over the three subunits and the trajectory. B) Deconstruction of the MPER-TMD1 residue contact map into individual helices. C) Number of interaction pairs between specific residues in the MPER-TMD2 simulation averaged over the three subunits and the trajectory. D) Deconstruction of the MPER-TMD2 residue contact map into individual helices.

Figure 7: Map of interactions between specific residues in the MPER-TMD simulations and the lipid membrane. Number of interaction pairs between residues in individual helices

and (A) lipid head group atoms and (B) lipid tail atoms. The y-axis denotes the simulation and subunit. It is worth noting that not all residues defined on the x-axis are present in all peptides (grey areas), and specifically residues 700-704 are lysine residues in MPER-TMD1. The grey box and arrows highlight the 10E8 epitope region and the most important residues.

Figure 8. Inter-helix interactions between protein residues in the MPER-TMD simulations. Number of interaction pairs between specific residues of individual helices in the A) MPER-TMD1$_{no\text{-}lys}$ simulation B) MPER-TMD1$_{C}$ simulation and C) MPER-TMD1$_{N}$ simulation.

Table 1. Average number of interactions of 10E8 epitope residues.

Simulation	Helix	Average Number of Inter-Helical Interactions						
		N671	W672	F673	T676	W680	K683	Total
MPER-TMD1	A	0	61	0	4	8	33	**106**
	B	0	0	0	0	0	8	**8**
	C	1	0	0	11	64	57	**131**
MPER-TMD2	A	9	41	1	6	2	35	**103**
	B	6	42	0	7	3	39	**97**
	C	0	28	0	0	1	32	**61**

Table 2. Average number of lipid interactions of 10E8 epitope residues

Simulation	Helix	Average Number of Lipid Interactions							
		N671	W672	F673	T676	W680	K683	Total	LIPID+ PROTEIN
MPER-TMD1	**A**	10	9	16	1	69	24	**129**	**235**
	B	2	41	50	25	117	48	**283**	**291**
	C	15	13	3	4	38	4	**77**	**208**
MPER-TMD2	**A**	0	0	7	2	95	33	**137**	**240**
	B	0	0	6	2	94	41	**143**	**240**
	C	0	1	11	6	92	44	**154**	**215**

Highlights

- 10E8 antibody neutralizes most HIV-1 strains; thus, it is target of vaccine design.
- 10E8 epitope exposure is analyzed in membrane-reconstituted MPER-TMD peptides.
- Immunochemical assays and Molecular Dynamics Simulation analyses are combined.
- TMD truncation at A700 destabilizes the reported trimer structure.
- A rational mutagenesis strategy is proposed to improve 10E8 epitope exposure.

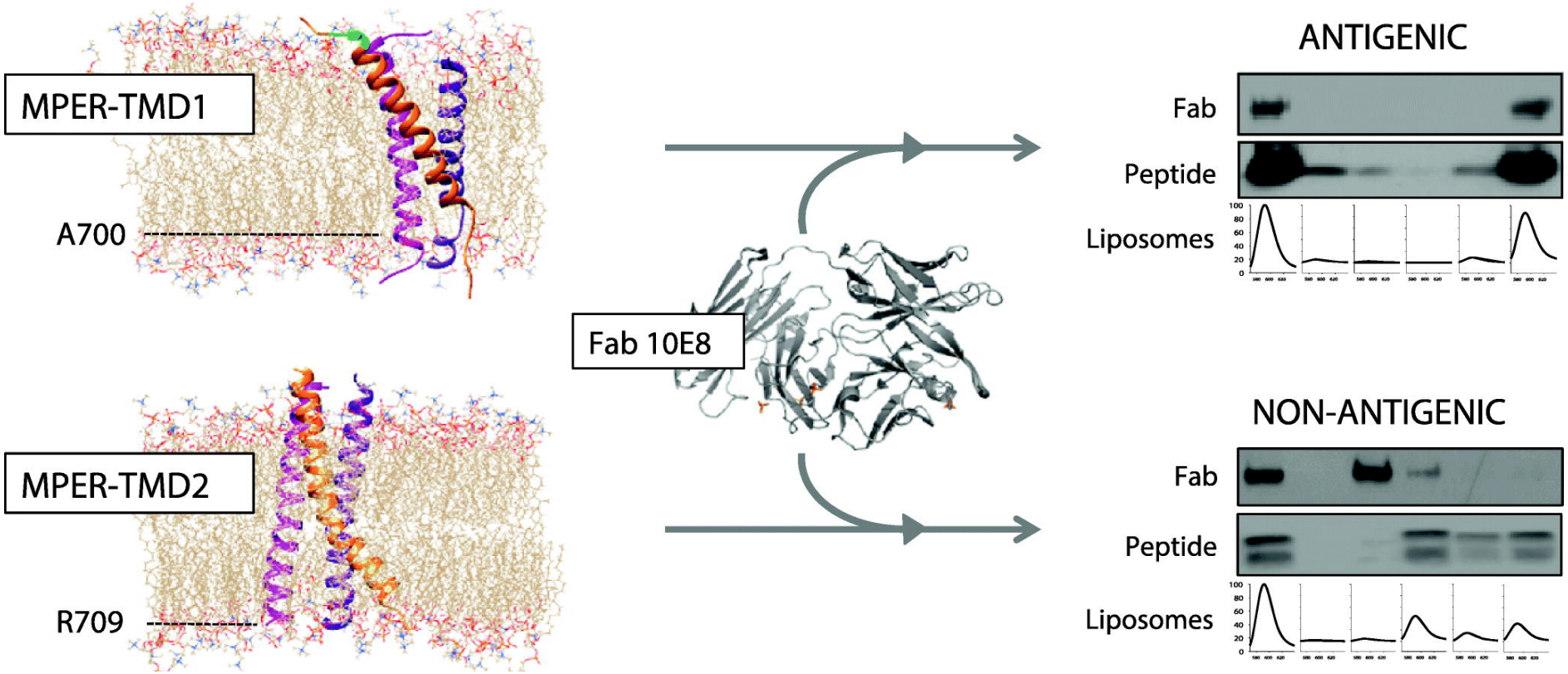

Graphics Abstract

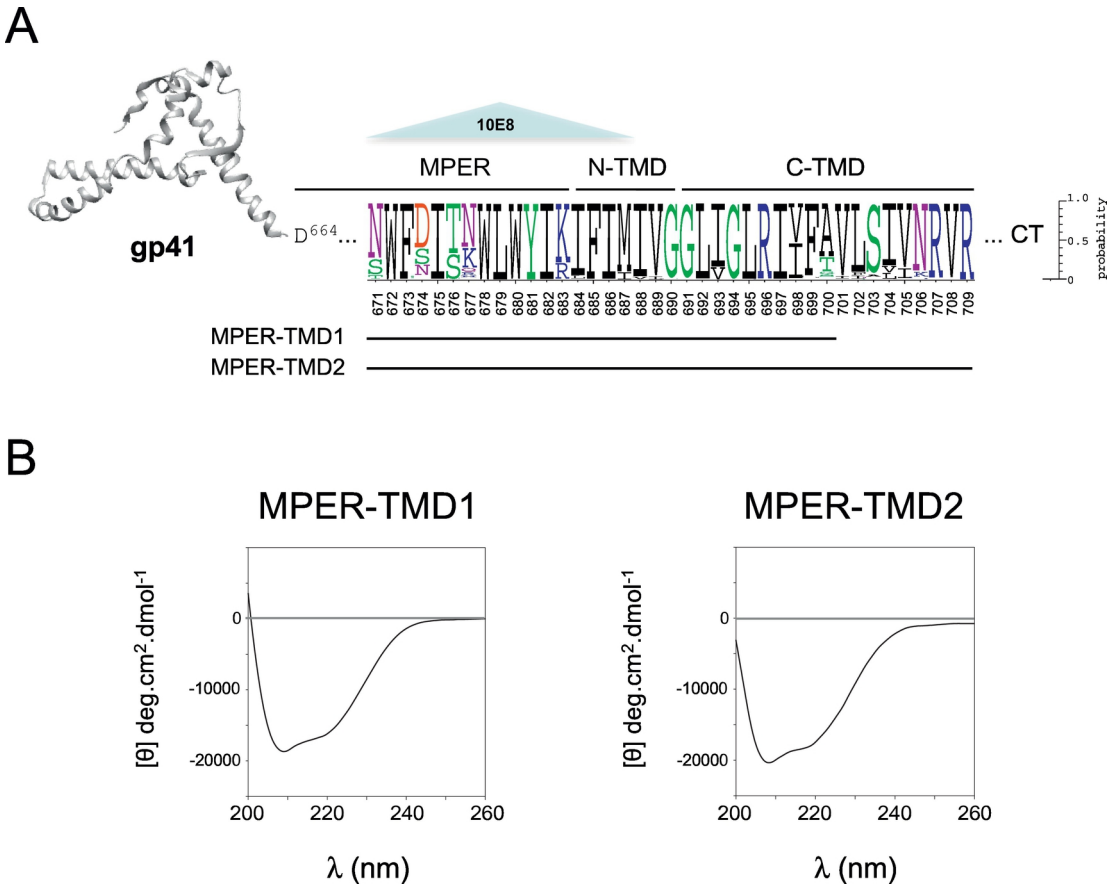
A
gp41
D664...
10E8
MPER
N-TMD
C-TMD
... CT
probability
1.0
0.5
0
671 672 673 674 675 676 677 678 679 680 681 682 683 684 685 686 687 688 689 690 691 692 693 694 695 696 697 698 699 700 701 702 703 704 705 706 707 708 709
MPER-TMD1
MPER-TMD2
B
MPER-TMD1
MPER-TMD2
[θ] deg.cm2.dmol-1
0
-10000
-20000
200 220 240 260
λ (nm)

Figure 1

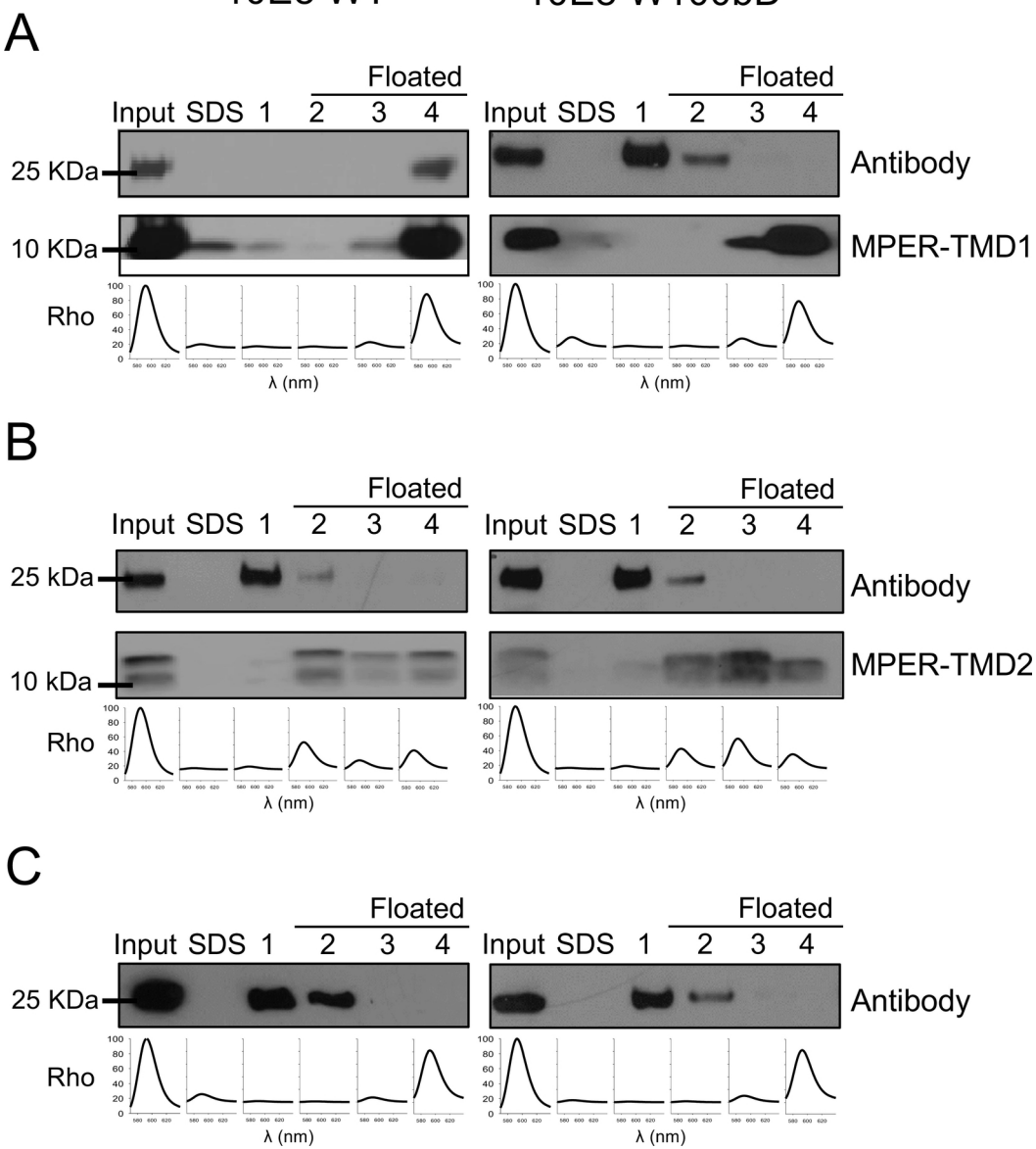
10E8 WT
10E8 W100bD
A
Floated
Input SDS 1 2 3 4
25 KDa
10 KDa
Rho
λ (nm)
Antibody
MPER-TMD1
B
25 kDa
10 kDa
MPER-TMD2
C

Figure 2

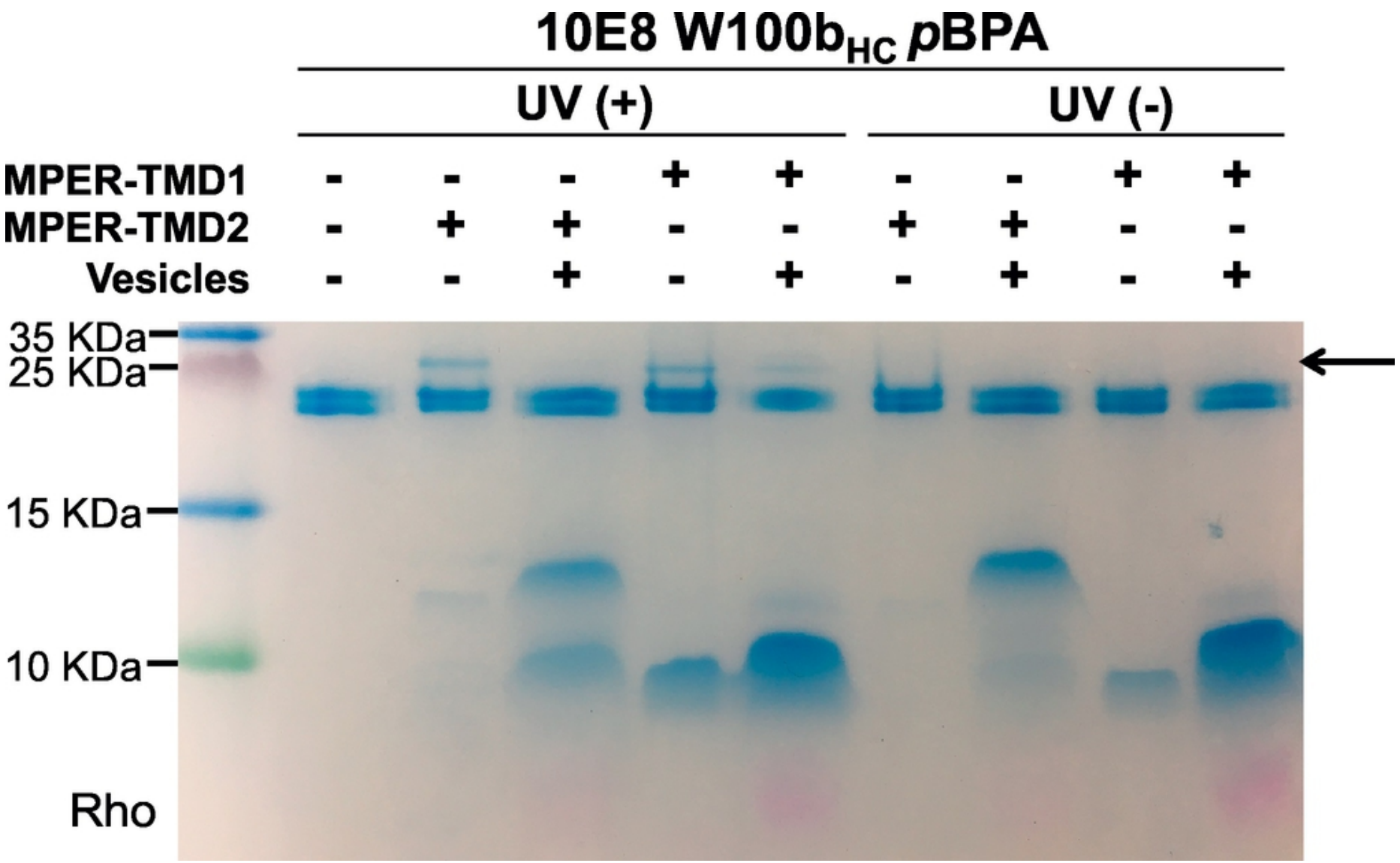
10E8 W100b$_{HC}$ pBPA
UV (+)
UV (-)
MPER-TMD1 - - - + + - - + +
MPER-TMD2 - + + - - + + - -
Vesicles - - + - + - + - +
35 KDa
25 KDa
15 KDa
10 KDa
Rho

Figure 3

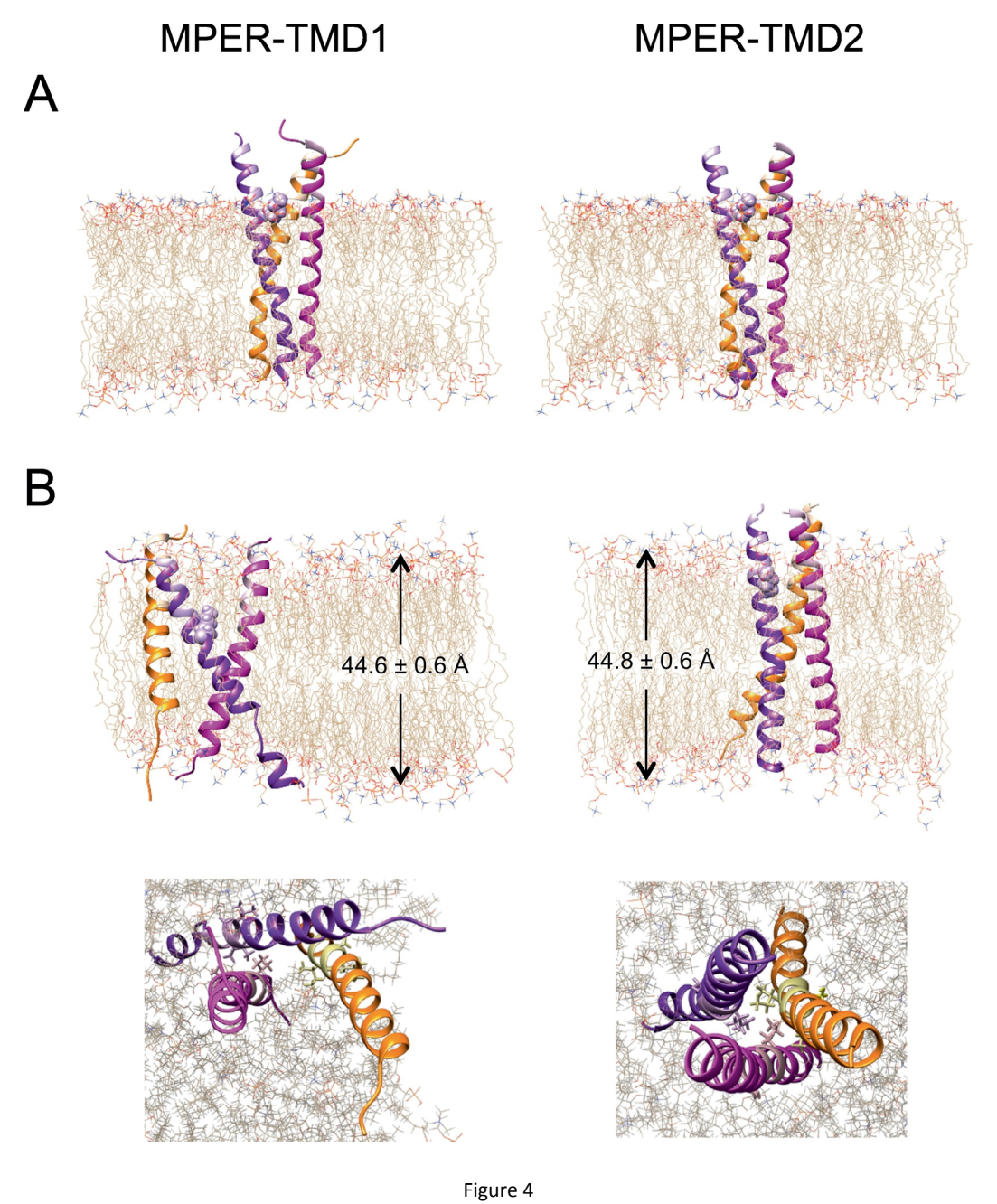

Figure 4

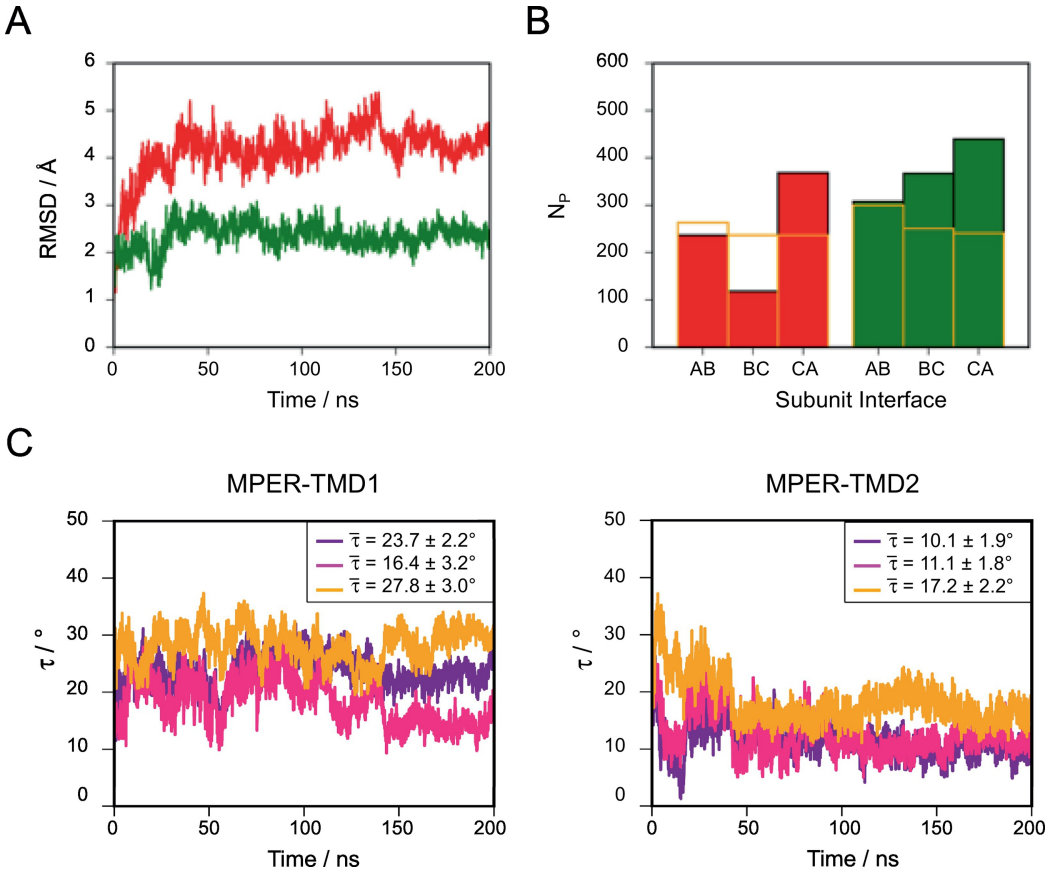
A
RMSD / Å
Time / ns
B
N_P
AB
BC
CA
AB
BC
CA
Subunit Interface
C
MPER-TMD1
$\overline{\tau}$ = 23.7 ± 2.2°
$\overline{\tau}$ = 16.4 ± 3.2°
$\overline{\tau}$ = 27.8 ± 3.0°
τ / °
Time / ns
MPER-TMD2
$\overline{\tau}$ = 10.1 ± 1.9°
$\overline{\tau}$ = 11.1 ± 1.8°
$\overline{\tau}$ = 17.2 ± 2.2°
τ / °
Time / ns

Figure 5

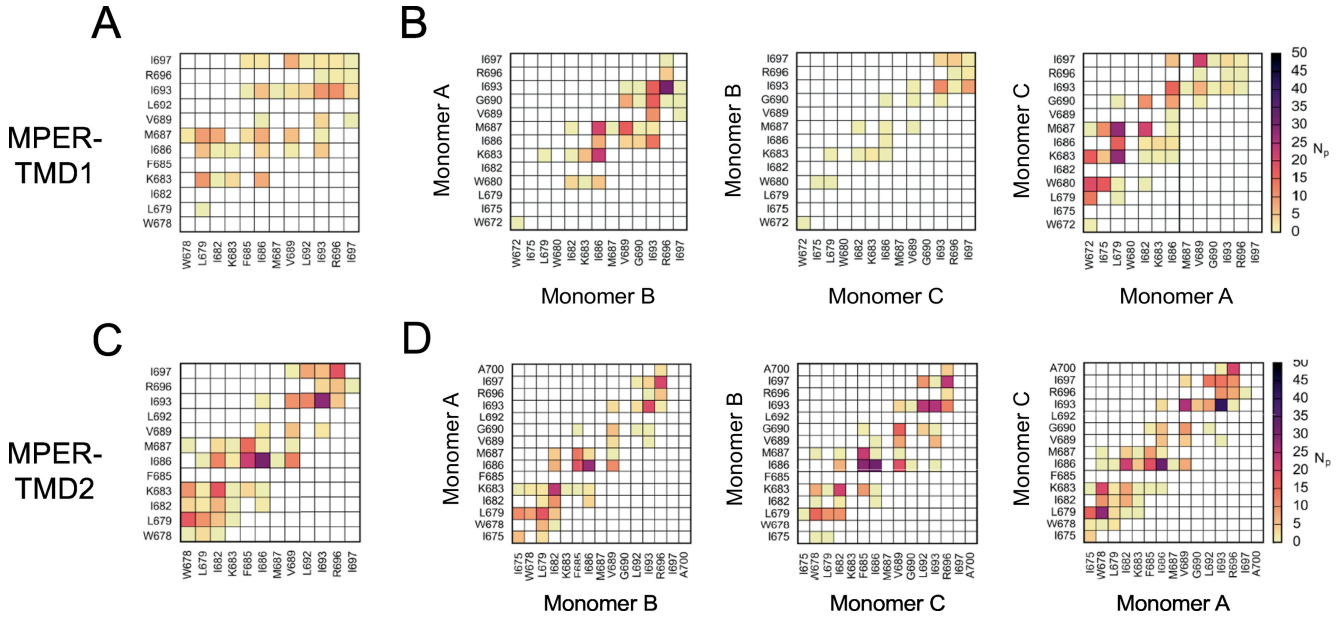
A
MPER-TMD1
B
Monomer A
Monomer B
Monomer C
Monomer B
Monomer C
Monomer A
C
MPER-TMD2
D
Monomer A
Monomer B
Monomer C
Monomer B
Monomer C
Monomer A
N_p

Figure 6

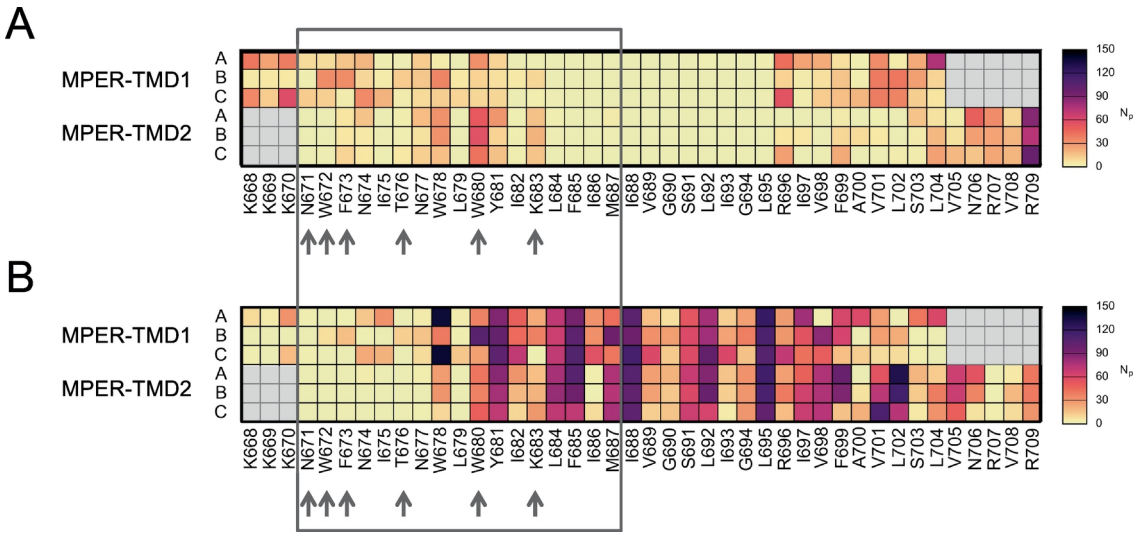
A
MPER-TMD1
MPER-TMD2
A
B
C
A
B
C
K668 K669 K670 N671 W672 F673 N674 I675 T676 N677 W678 L679 W680 Y681 I682 K683 L684 F685 I686 M687 I688 V689 G690 S691 L692 I693 G694 L695 R696 I697 V698 F699 A700 V701 L702 S703 L704 V705 N706 R707 V708 R709
150
120
90
60
30
0
N_p
B
MPER-TMD1
MPER-TMD2
A
B
C
A
B
C
K668 K669 K670 N671 W672 F673 N674 I675 T676 N677 W678 L679 W680 Y681 I682 K683 L684 F685 I686 M687 I688 V689 G690 S691 L692 I693 G694 L695 R696 I697 V698 F699 A700 V701 L702 S703 L704 V705 N706 R707 V708 R709
150
120
90
60
30
0
N_p

Figure 7

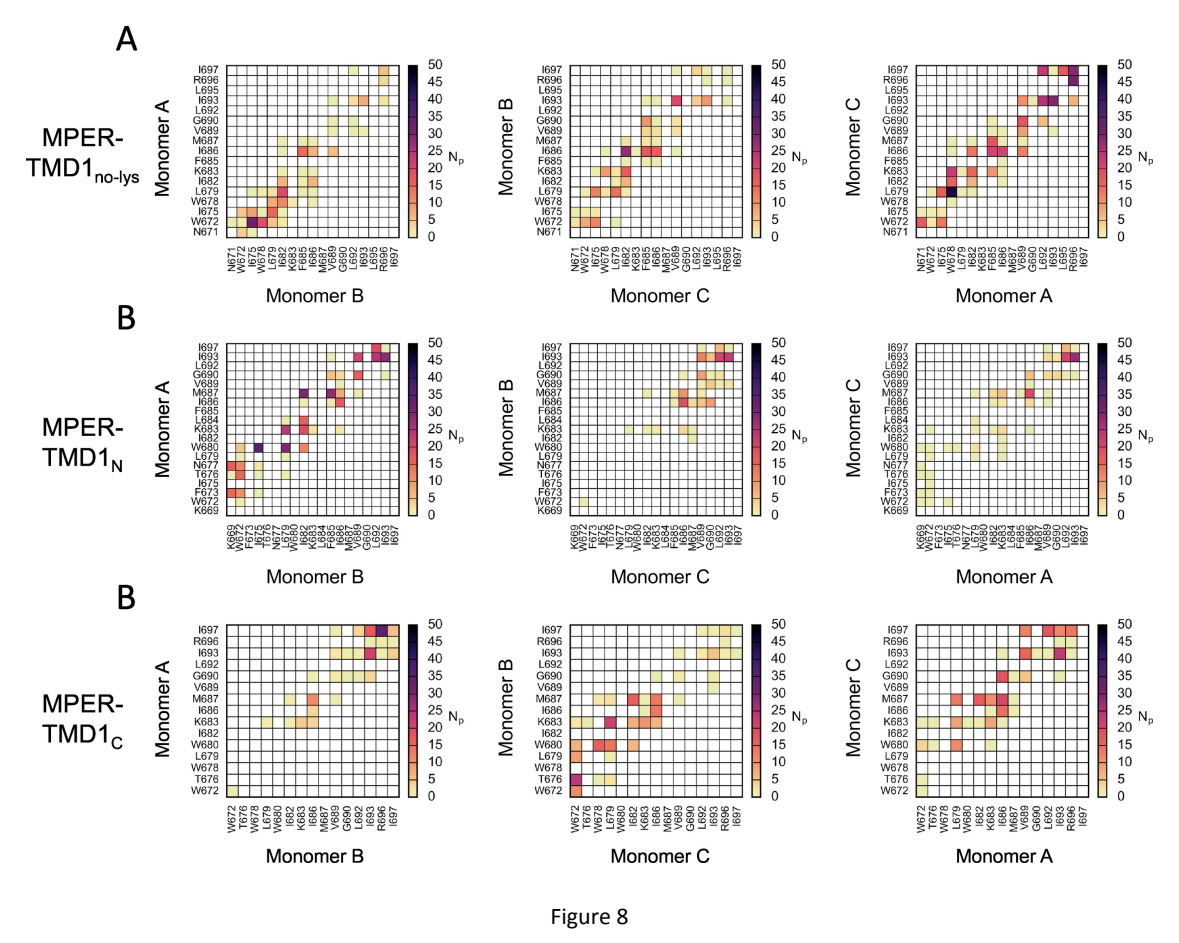
A
MPER-TMD1no-lys
Monomer A
Monomer B
Monomer C
Np
B
MPER-TMD1N
Monomer A
Monomer B
Monomer C
Np
B
MPER-TMD1C
Monomer A
Monomer B
Monomer C
Np

Figure 8